แอนไอออนเซ็นเซอร์ที่มีอนุพันธ์ของอิมิดาโซลและแอนทราควิโนนเป็นองค์ประกอบ

นางสาว มัชฌิมา มโนวงค์

วิทยานิพนธ์นี้เป็นส่วนหนึ่งของการศึกษาตามหลักสูตรปริญญาวิทยาศาสตรมหาบัณฑิต
สาขาวิชาเคมี   ภาควิชาเคมี
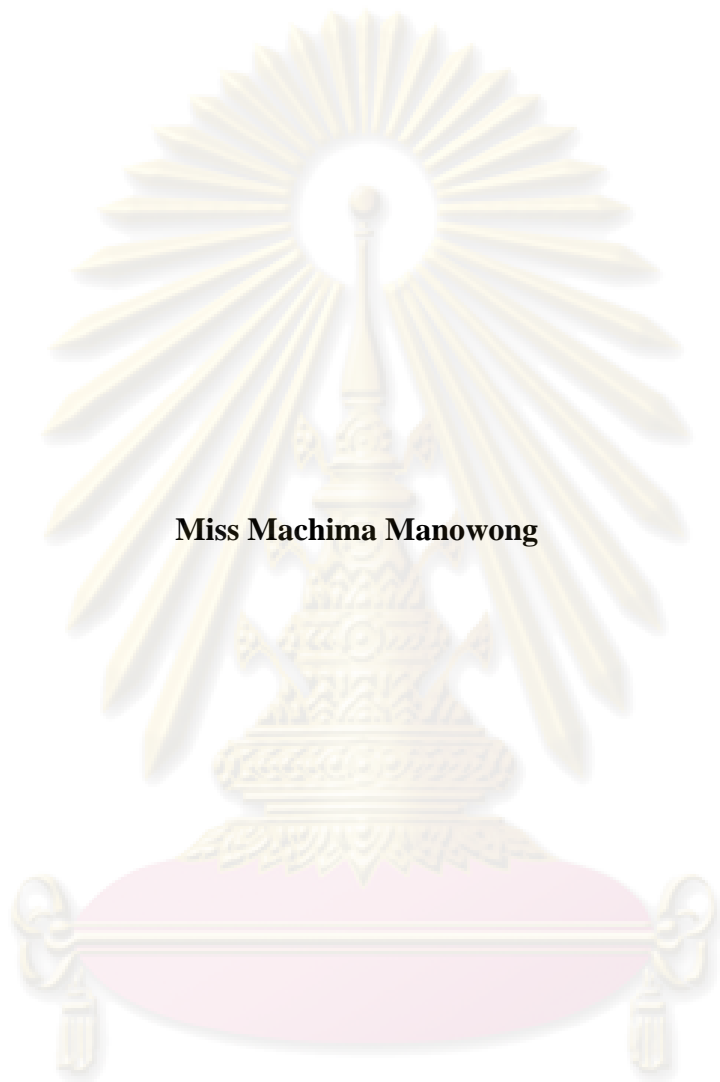คณะวิทยาศาสตร์ จุฬาลงกรณ์มหาวิทยาลัย
ปีการศึกษา 2551

ANION SENSORS CONTAINING IMIDAZOLE AND ANTHRAQUINONE

DERIVATIVES

Miss Machima Manowong

**A Thesis Submitted in Partial Fulfillment of the Requirements
for the Degree of Master of Science Program in Chemistry
Department of Chemistry
Faculty of Science
Chulalongkorn University
Academic Year 2008**

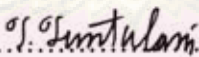|	
Thesis Title	ANION SENSORS CONTAINING IMIDAZOLE AND ANTHRAQUINONE DERIVATIVES
By	Miss Machima Manowong
Field of Study	Chemistry
Thesis Principal Advisor	Associate Professor Thawatchai Tuntulani, Ph.D.
Thesis Co-advisor	Assistant Professor Boosayarat Tomapatanaget, Ph.D.

Accepted by the Faculty of Science, Chulalongkorn University in Partial Fulfillment of the Requirements for the Master's Degree
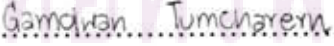
.... Dean of the Faculty of Science

(Professor Supot Hannongbua, Dr.rer.nat.)
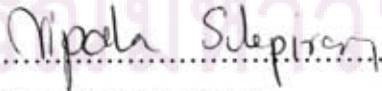
Thesis Committee

....Chairman

(Professor Udom Kokpol, Ph.D.)

....Thesis Principal Advisor

(Associate Professor Thawatchai Tuntulani, Ph.D.)

....Thesis Co-advisor

(Assistant Professor Boosayarat Tomapatanaget, Ph.D.)

....External Member

(Gamolwan Tumcharern, Ph.D.)

....Member

(Nipaka Sukpirom, Ph.D.)

มัชฌิมา มโนวงศ์: แอนไอออนเซ็นเซอร์ที่มีอนุพันธ์ของอิมิดาโซลและแอนทราควิโนนเป็นองค์ประกอบ. (ANION SENSORS CONTAINING IMIDAZOLE AND ANTHRAQUINONE DERIVATIVES) อ.ที่ปรึกษาวิทยานิพนธ์หลัก: รศ.ดร. ธวัชชัย ตันทุลานิ, อ.ที่ปรึกษาวิทยานิพนธ์ร่วม: ผศ.ดร. บุษยรัตน์ ธรรมพัฒนกิจ, 76 หน้า.

ได้ดัดแปลงคาร์บอนนาโนทิวบ์ชนิดผนังร้อนด้วยอนุพันธ์ของแอนทราควิโนนที่มีอิมิดาโซเลียมเป็นองค์ประกอบ จากนั้นศึกษาสมบัติในการเกิดสารประกอบเชิงซ้อนกับแอนไอออนชนิดต่างๆ ได้แก่ ฟลูออไรด์ คลอไรด์ โบรไมด์ ไอโอไดด์ และไดไฮโดรเจนฟอสเฟต และกรดอะมิโน ได้แก่ ไกลซีน ดีอะลานีน ดีลิวซีน ดีฟีนิลอะลานีน และดีทริบโตฟาน ด้วยเทคนิคไซคลิกโวแทมเมทรีในสารละลายบัฟเฟอร์ pH 7 (HEPES + NaCl) พบว่าไม่เกิดการเปลี่ยนแปลงกับทั้งแอนไอออนและกรดอะมิโน แต่อนุพันธ์ของคาร์บอนนาโนทิวบ์ที่เกาะบนผิวของกลาสซีคาร์บอนอิเล็กโทรดแสดงคุณสมบัติเด่นในการเป็นตัวเร่งปฏิกิริยาออกซิเดชันของไฮดราซีน โดยกระแสไฟฟ้าที่วัดได้เพิ่มขึ้นเป็นสัดส่วนโดยตรงกับความเข้มข้นของไฮดราซีน ค่าความเข้มข้นต่ำสุดของไฮดราซีนที่สามารถวัดได้ (LOD) เท่ากับ 1.01 ไมโครโมลาร์ ซึ่งคำนวณได้จากกราฟมาตรฐานที่พล็อตระหว่างกระแสไฟฟ้าและความเข้มข้นของไฮดราซีนในช่วง 0.0 ถึง 10.0 ไมโครโมลาร์ และในงานวิจัยนี้ได้เสนอกลไกในการเกิดปฏิกิริยาระหว่างอนุพันธ์ของคาร์บอนนาโนทิวบ์และไฮดราซีน

ภาควิชา............เคมี.............. ลายมือชื่อนิสิต.............มัชฌิมา มโนวงศ์...........
สาขาวิชา............เคมี.............. ลายมือชื่อ อ.ที่ปรึกษาวิทยานิพนธ์หลัก....ธวัชชัย ศพาทุลาทิ
ปีการศึกษา........2551.............. ลายมือชื่อ อ.ที่ปรึกษาวิทยานิพนธ์ร่วม....บุษยรัตน์ ธรรมบงค

4872417823: MAJOR CHEMISTRY

KEY WORDS: ANTHRAQUINONE / IMIDAZOLE / CARBON NANOTUBES / GLASSY CARBON ELECTRODE / CYCLIC VOLTAMMETRY / SENSOR

MACHIMA MANOWONG: ANION SENSORS CONTAINING IMIDAZOLE AND ANTHRAQUINONE DERIVATIVES. THESIS PRINCIPAL ADVISOR: ASSOC. PROF. THAWATCHAI TUNTULANI, Ph. D., THESIS CO-ADVISOR: ASST. PROF. BOOSAYARAT TOMAPATANAGET, Ph. D., 76 pp.

An anthraquinone derivative containing imidazolium salt **L1** was synthesized and then covalently attached to the surface of multi-walled carbon nanotubes. Complexation studies of the modified nanotubes supported on glassy carbon electrodes with anions including F^-, Cl^-, Br^-, I^-, and $H_2PO_4^-$ and amino acids, such as glycine, D-alanine, D-leucine, D-phenylalanine and D-tryptophan were carried out by cyclic voltammetry. However, no changes in CV were observed. Conversely, the prepared electrodes showed promising electrocatalytic activities for hydrazine oxidation. The catalytic behavior of the reaction between **L1** modified nanotubes acting as a mediator and hydrazine was analyzed by cyclic voltammetry in pH 7.0 buffer solution (HEPES + NaCl). It was found that the catalytic currents proportionally increased to the concentration of hydrazine, leading to calibration plots for the determination of hydrazine. The modified electrode as a hydrazine sensor exhibited the detection limit 1.01 µM obtaining from the linear range over hydrazine concentration 0.0-10.0 µM. Herein, we proposed the mechanism of the electrocatalytic oxidation of hydrazine at glassy carbon electrodes functionalized with **L1/MWNTs**.

ศูนย์วิทยทรัพยากร

จุฬาลงกรณ์มหาวิทยาลัย

Department:.......Chemistry...... Student's signature.........Machima....Manowong..........

Field of study:.....Chemistry...... Principal Advisor's signature...T. Tuntulani.............

Academic year:......2008.......... Co-advisor's signature........Boonyarat...Rompatmagt....

ACKNOWLEDGEMENTS

ศูนย์วิทยทรัพยากร
จุฬาลงกรณ์มหาวิทยาลัย

CONTENTS

LIST OF TABLES

LIST OF FIGURES

ศูนย์วิทยทรัพยากร
จุฬาลงกรณ์มหาวิทยาลัย

LIST OF SCHEMES

LIST OF ABBREVIATIONS AND SYMBOLS

A	Ampere
°C	Degree Celsius
DIC	Diisopropylcarbodiimide
Durapore DVPP	Poly(vinylidene fluoride)
Eq.	Equation
g	Gram
^{1}H-NMR	Proton nuclear magnetic resonance
Hz	Hertz
J	Coupling constant
L	Litre
μ	Micro
m	Milli
M	Molar
n	Nano
ppm	Part per million
s	Second
δ	Chemical shift
s, d, t, m	Splitting patterns of ^{1}H-NMR (singlet, doublet, triplet, multiplet)
V	Volt
TEM	Transmission electron microscopy

CHAPTER I

INTRODUCTION

1.1 Hydrazine

1.1.1 General Characteristics and Applications

Hydrazine, clear and colorless liquid, is a highly active base and reducing agent which has been widely applied in many industrial and pharmaceutical fields. The principle uses for hydrazine are as an intermediate in the synthesis of maleic hydrazide and in the manufacture of chemical blowing agents that are used in the plastics production. Hydrazine applications also include using as a corrosion inhibitor, a water treatment agent, a rocket propellant, a polymerization catalyst, a scavenger for gases, along with a medication for sickle cell anemia and cancer.

1.1.2 Toxicity

Hydrazine can be directly released into water, soil and air. People can be exposed to hydrazine by breathing, eating, drinking or skin contact. The severity of health effects will be determined by many factors, such as the dose, the duration, the pathway of exposure and individual characteristics, e.g. age, sex, nutritional status and the state of health. An odor threshold is typically 3.7 ppm.

Although hydrazine appears widespread usages in commercial manufactures, the harmful effects in people have not been well studied. Some case studies suggest that lung, liver, kidney and central nervous system may be injured if people breathe in hydrazine or get exposed by skin contact, and animals have also been affected in a similar way. Sometimes those of effects found in animals may include the change of biochemical substances on the liver [1] and the decrease of ovary size or sperm production. After being oral exposed to hydrazine, people possibly experience stomachache, vomiting, uncontrolled shaking, lethargy, coma, and an inflammation of nerves. Furthermore, there are some studies indicating that hydrazine can cause cancer in some animals. Tumors have normally been found in lungs, blood vessels

and colons. However, there are few pieces of evidence of the cancer-caused effects in human. The mortalities from lung cancer, cancer of digestive system and other cancers were observed among men working at a hydrazine plant, but it is a long-term effect [2].

1.2 Carbon Nanotubes

1.2.1 General Characteristics and Applications

A carbon nanotube is considered as a long cylinder consisting of one or more seamless shells of graphene sheets and capped by hemispherical ends. The combination of a pentagon and five surrounding hexagons results in the topological curvature to completely enclose the hexagonal lattice. Similar to graphite, carbon atoms in the nanotubes form sp^2 hybridized type of bonding and one electron is allowed to delocalize among the surface. Nevertheless, the circular curvature will cause quantum confinement and σ-π rehybridization in which three σ bonds are slightly out of plane; therefore, the π orbital is more delocalized outside the tube. According to this reason, it gives rise to higher electrical and thermal conductivity than graphite [3]. The nanotubes also show high tensile strength and stiffness, a large Young's modulus indicating the elasticity, and high surface area [4].

CNTs typically form in two main categories: multi-walled carbon nanotubes (MWNTs) and single-walled carbon nanotubes (SWNTs) [5]. The MWNTs were firstly discovered by Iijima in 1991 while he was studying the synthesis of fullerene by an arc-discharge evaporation method [6]. This type of nanotubes comprises of several coaxial tubes with a hollow core. The interlayer distance is close to a spacing between the layers in graphite (0.34 nm), but slightly higher than SWNTs (0.335 nm). A diameter of MWNTs is in a range of 2 to 100 nm. The single-walled carbon nanotube is a rolled-up tube of graphene sheet with the typical diameter ~1 nm. During the rolling up of graphene layers, the translation shift along the edges may occur in order to obtain the best fit between the layers, leading to a different orientation of the lattice. Therefore, it is generally found different helical systems (helicity) of hexagonal shells in the tubular structure. Depending on the diameter and the helicity of the tubes, the CNTs can be either metallic or semiconducting [7].
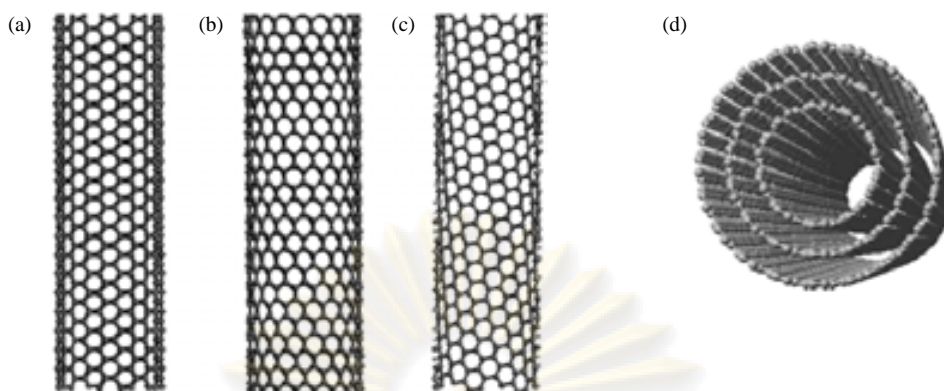
Figure 1.1 Single-walled carbon nanotubes with different helicities, (a) armchair, (b) zigzag and (c) chiral structure. The graphene sheets rolled up into concentric cylinders form MWNTs (d).

Although the nanotubes appear in a form of seamless cylinder, it is noteworthy that they may contain defects categorized into three types: topological defects, rehybridization defects and incomplete bonding. Instead of hexagons, the presence of other rings (normally a pair of pentagon-heptagon) in the structure is topological defect which causes slightly changes of the diameter and the helicity of the tubes. In case of rehybridization defect, it seems likely that the pentagons at the end caps induce the tubular material to grow with a polygonal structure instead of a cylindrical shape. Finally, incomplete bonding is one derived from the translation of the edges; however, it is rarely found in normal arc-produced samples [8].

In regard to the outstanding properties of high conductivity, high mechanical strength, chemical inertness and large surface area, CNTs can be considered as promising material in nanotechnological applications. Nevertheless, as-received CNTs are insoluble in all aqueous and non-aqueous systems. The lack of solubility leading to the difficult manipulation in any solvents has restricted the usage of CNTs in various fields. To facilitate their integration into organic, inorganic and biological systems, the chemical functionalizations via covalent and non-covalent are required.

1.2.2 The Modification of Carbon Nanotubes

The covalent chemical modification has been typically based on the oxidation reactions introducing carboxyl groups at the end caps and the defect sites of CNTs, which can be processed by a number of approaches, such as nitric treatment [9-10], combined sulfuric and nitric acids treatment [11], treatment with $KMnO_4$ [12], chemical oxidation with Piranha solutions [13] and ozonolysis [14]. The oxidative strategies can generate various oxygen-based functional groups, e.g. aldehyde, ketone, alcohol and carboxylic groups that are capable of forming amide [15] and ester [16] linkages in the further reactions.

The non-covalent functionalization that usually dominates π-π stacking interaction between cyclic compounds and the tube surface becomes the promising approach, because it preserves the unique electrical and mechanical characteristics of CNTs [17-18]. As a result of the immobilization with proper substances, the solubility of modified nanotubes increases [19-21], resulting in diverse fields of electrochemical sensors [22-26], biosensors [27-30], nanomaterial [31] and medicine [32].

1.2.3 The Electrocatalytic Properties of MWNTs Modified Electrodes toward Hydrazine Oxidation

As mentioned above, hydrazine has been widely used in various applications, and also causes toxicities to animals and human being. The highly sensitive methods and the reliable measurements are then required for hydrazine detection at low level. It has been shown that the oxidation of hydrazine is very active at Au [33] and Pt electrodes [34]; however, these are too expensive for practical applications. In addition, hydrazine oxidation at conventional carbon electrodes generally occurs at the large overpotential which is not appropriate for quantitative analysis. To overcome these overvoltage effects, it is highly desirable to immobilize electrodes with specific redox mediators through the chemical modifications. There are a number of studies reporting the electrocatalytic oxidation of hydrazine at glassy carbon electrodes fabricated with hematoxylin [35], pyrogallol red [36], iron hexacyanoferrate [37], overoxidized polypyrrole [38] and quinizarine [39].

Nassef and coworkers reported the simply covalent modification of glassy carbon electrode with *o*-aminophenol grafted film. The modified electrode was

obtained by the electrochemical reduction of nitrophenyl diazonium salt in acidic aqueous solution. The electrocatalytic behavior of the grafted *o*-aminophenol electrode as a mediator for hydrazine oxidation was characterized by cyclic voltammetry, chronoamperometry and rotating disk electrode voltammetry. In the presence of hydrazine (200 µM), the modified electrode exhibited considerable response (Figure 1.2(b) curve b) toward hydrazine oxidation compared with bare GC electrode (Figure 1.2(b) curve d), which can be schematically illustrated by Figure 1.2(a). The detection limit of 0.5 µM was obtained from a calibration plot between an anodic current and hydrazine concentration [40].
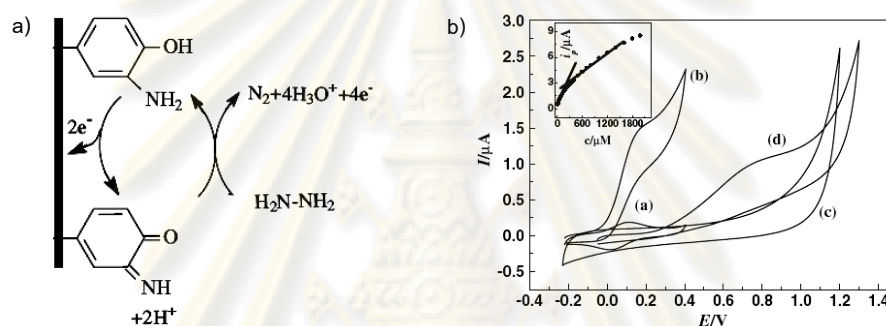
Figure 1.2 Schematic diagram for electrocatalytic oxidation of hydrazine at *o*-AP modified GC electrode (a). Cyclic voltammograms (b) of *o*-AP modified (curve a,b) and bare (curve c,d) GC electrodes in the absence (curve a,c) and in the presence (curve b,d) of 200 µM hydrazine.

1.3 Anthraquinone

1.3.1 General Characteristics of Anthraquinone

Anthraquinone, or more correctly anthra-9,10-quinone, is a member of quinone compounds which can be defined as cyclohexadienedione. It represents the characteristic system of three linear fused six-membered rings in which the center contains two carbonyl groups. Anthraquinone and its derivatives have been spread out in a large number of dye applications. We can find numerous anthraquinone dyes in nature, but at present the synthetic anthraquinone colorants are the most significant. Many of the current commercial range of synthetic anthraquinone dyes are simply substituted derivatives of anthraquinone system [41].

The quinone-hydroquinone system represents the characteristic of a reversible redox system involving the stepwise transfer of two-electron electrochemical reductions. In general, these redox reactions are carried out in alkaline media, in which the unprotonated semiquinone is first formed and the dianion is the final reduction product. The reduction of anthraquinone to hydroquinone can be illustrated by Figure 1.3 [41-42].

anthraquinone   semiquinone   dianion
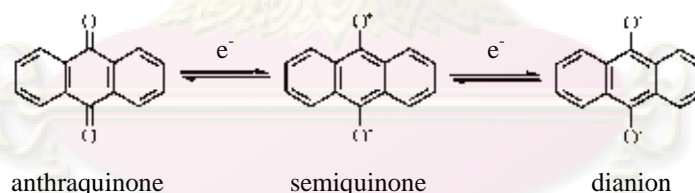
Figure 1.3 The redox reaction of anthraquinone-hydroquinone system.

1.3.2 Molecular Sensors Based on Anthraquinone Group

A molecular sensor is typically defined as the system consisting of the binding part and the signaling unit. The binding site or receptor can be any of systems such as amide, urea, thiourea, pyrrole, crown ethers and cryptands etc., which must be selective for the target analyte. The signaling unit which is connected to the receptor will convert the recognition phenomena to a signal in the form of a current, a color, or any measurable changes [43].

Due to the unique characteristics of quinoid structure, anthraquinone derivatives have been commonly used as a chromophore and electrochemical signaling unit in the field of molecular sensors.

Devaraj and coworkers studied the properties of anthraquinone-based receptors toward fluoride ion. Three receptors with different substituents were synthesized by Schiff's base condensation. The dramatic color changes of all receptors were observed in the presence of F^- whereas those of receptors were not sensitive to the addition of a large excess of Cl^-, Br^- and I^-. It was proposed that hydrogen bonding between OH group and F^- incorporating charge-transfer between fluoride ion and anthraquinone part induced the changes of color. Furthermore, the recognition behavior of all receptors toward halide anions was carried out by cyclic voltammetry. The successive addition of F^- gave rise to decreasing of the cathodic peak current along with the cathodic shift, implying the strong interaction of the synthesized compound and fluoride ion [44].
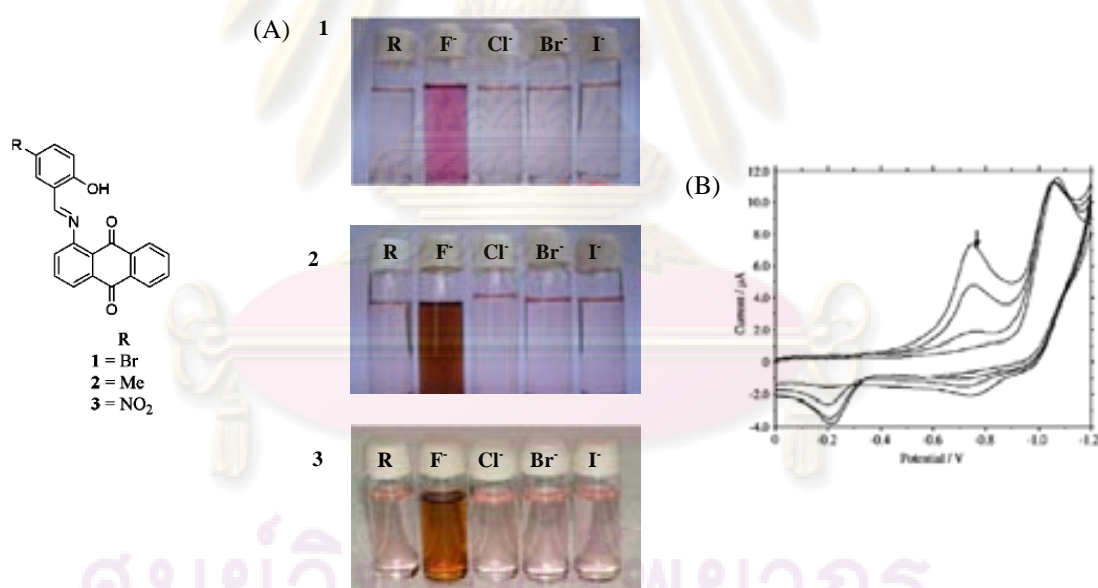
Figure 1.4 Color changes of receptor (R) **1-3** in DMSO (A). Cyclic voltammograms of **1** in DMSO (5.0×10^{-5}) upon addition of tetrabutylammonium fluoride (B).

Moreover, Bang *et al*. reported the simply chemical derivatisation of multi-walled carbon nanotubes with 1-anthraquinonyl group (AQ-MWNTs) and then fabricated to basal plane pyrolytic graphite electrode (bppg). The modified electrode was employed to mediate the electrocatalytic reduction of oxygen investigated by voltammetric measurements. In comparison to bare graphite electrode (Figure 1.5(A) curve B), the electrode attached with anthraquinone/carbon nanotubes (Figure 1.5(A) curve C) exhibited a significant shift to less negative potential with increasing of the current in a saturated oxygen solution, which suggested the effective electrocatalytic activity for the oxygen reduction [45]. The mechanism of the electrocatalytic reduction of oxygen was depicted in Figure 1.5(B).
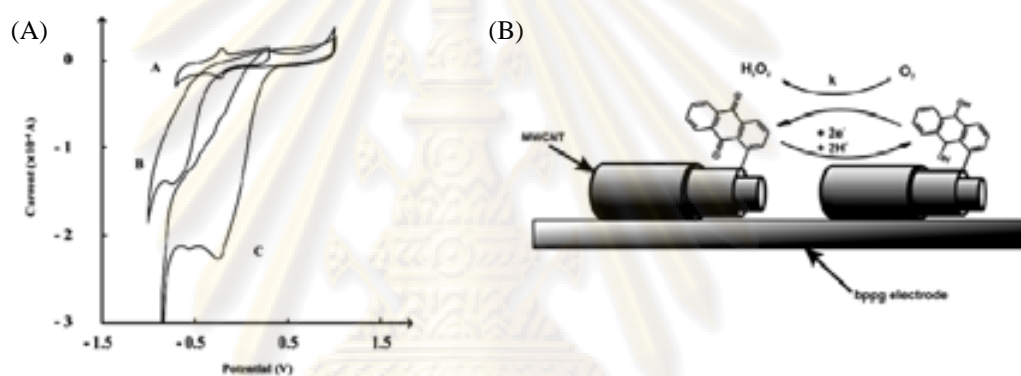
Figure 1.5 Cyclic voltammograms of (A) AQ-MWNTs attached to graphite electrode (curve A), bare graphite electrode in a saturated oxygen solution (curve B), AQ-MWNTs in a saturated oxygen solution (curve C). Schematic representation of anthraquinone modified MWNTs on a basal plane pyrolytic graphite electrode showing the mechanism of the electrocatalytic reduction of oxygen (B).

1.4 Anion Receptor Based on Imidazolium Group

Nowadays, selective recognition and sensing of anions by artificial receptors have attracted considerable interest because of their applications in large areas of chemistry, biochemistry and medicine. In order to achieve high recognition, it is desirable that an artificial receptor must be organized to perfectly complement the analyte in term of size, shape and chemical properties, etc. A variety of functional groups, such as amide, urea/thiourea, guanidinium and polyammonium have been generally employed as a binding unit [46]. Imidazolium moiety is one of the

positively charged derivatives that has been developed for anion recognition because it can coordinate with anions through $(C-H)^+\cdots X^-$ charged hydrogen bonding.

Yoon *et al.* synthesized anthracene dimer bearing two imidazolium moieties and reported the selective recognition of $H_2PO_4^-$ by forming $(C-H)^+\cdots X^-$ ionic hydrogen bond between imidazolium part and anion. ^{1}H NMR spectra showed the significant changes after the addition of excess $H_2PO_4^-$ suggesting the complexation between the synthesized ligand and $H_2PO_4^-$. Moreover, the fluorescence emission changes upon adding $H_2PO_4^-$ were observed and the fairly large association constant was obtained [47].
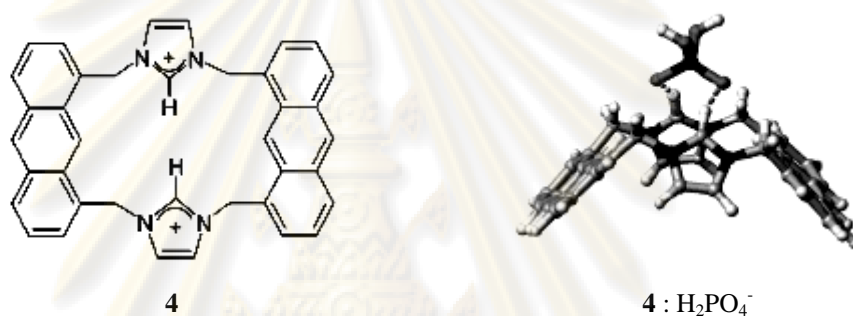
4   **4** : $H_2PO_4^-$

Figure 1.6 The structure of **4** and the optimized geometry of **4** : $H_2PO_4^-$ complex

1.5 Electrochemical Sensors

Chemical sensors are considered as molecules that are able to bind selectively with the target analyte, resulting in the changes of the system properties, such as redox potentials, and/or absorption or luminescence spectra. Two processes including molecular recognition and signal transduction are required to obtain the detection of the analyte of interest. Thus, chemosensors are typically comprised of three units: a receptor, an active unit and the spacer, which is schematically illustrated by Figure 1.7.

Electrochemical sensors are considered as the subclass of chemical sensors, which exploit the powerful of electrochemical methods and the selectivity of chemical recognition processes. They have shown a wide range of applications in the fields of clinical and medical sciences, biochemistry, environmental analysis and analytical chemistry. For electrochemical sensors, the molecular recognition will be transformed to electrical signals, amperometric or potentiometric response.
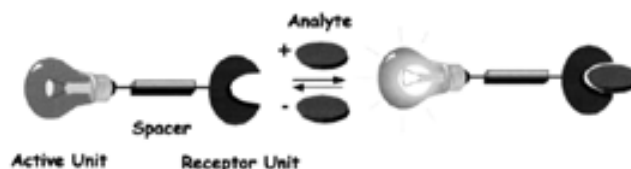
Figure 1.7 Representation of general chemosensors [48].

1.6 Electrochemistry

Electrochemistry is the science of electron transfer across a solution-electrode interface, which is concerned between electricity and chemistry. Because electrical measurements appear as portable and inexpensive methodologies, including sensitive and selective properties, thus they have played an important role in analytical chemistry. Electroanalytical techniques can be categorized into two types, potentiometric and potentiostatic [49]. Potentiometry is a static (zero current) technique in which the potential established at the electrode-solution interface is measured. Potentiostatic or controlled-potential techniques are dynamic (no current zero) approaches that an electron-transfer reaction is forced by the applied potential, and then the resultant current is measured.

1.6.1 Cyclic Voltammetry

Cyclic voltammetry has been widely used for qualitative purposes, such as study of redox processes, reaction mechanisms and kinetics of electron transfer processes. This technique is based on varying the applied potential at a working electrode in both forward and backward directions while monitoring the resultant current. The potential applied to the working electrode is in a triangular waveform shown in Figure 1.8. Depending on the analysis, one full cycle, a partial cycle, or a series of cycles can be performed. The corresponding plot of current versus potential is termed cyclic voltammogram.
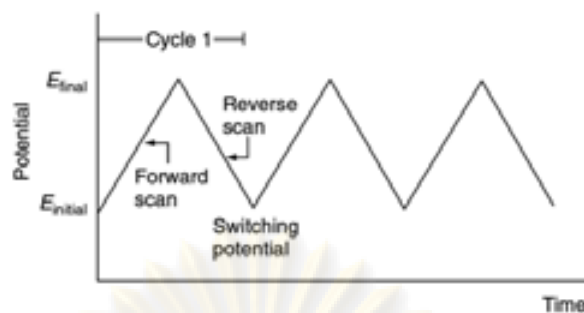
Figure 1.8 Potential-time excitation signal in cyclic voltammetry experiment.

1.6.1.1 Reversible Systems

In general case studies, both reversible and irreversible processes can be found. The response of a reversible redox couple is illustrated by Figure 1.9. Firstly, the oxidized form of O is reduced by a negative potential scan in forward direction, starting from a value where no reduction occurs. When the applied potential arises the characteristic $E°$ for the redox process, a cathodic current begins increasing. At the switching potential, the scan would be reversed and run in the positive scan, in which R molecules are reoxidized back to O and provides an anodic current.
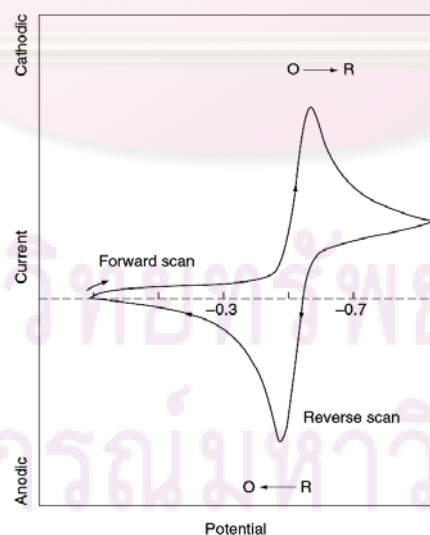
Figure 1.9 Typical cyclic voltammetry for reversible O + ne⁻ ⇌ R redox process.

For a reversible reaction, the correlation between the peak current and the concentration is expressed by the Randles-Sevcik equation (25°C):

$$i_p = (2.69 \times 10^5)\, n^{3/2}\, ACD^{1/2}\, v^{1/2} \tag{1}$$

where i_p is the peak current in amps, A is the electrode area (in cm^2), C is the concentration (in mol cm^{-3}), D is the diffusion coefficient (in cm^2 s^{-1}), and v is the scan rate (in V s^{-1}).

The formal reduction potential ($E°$) is related to the position of the peaks on the potential axis (E_p) given by

$$E° = \frac{E_{p,a} + E_{p,c}}{2} \tag{2}$$

In addition, the number of electrons involving in the redox couple can be obtained from the separation between the peak potentials shown as Eq. (3), or about 60 mV for one electron. However, it is difficult to obtain this value in practical experiments due to such factors as cell resistance.

$$\Delta E_p = E_{p,a} - E_{p,c} = \frac{0.059}{n}\,\text{V} \tag{3}$$

1.6.1.2 Irreversible and Quasi-Reversible systems
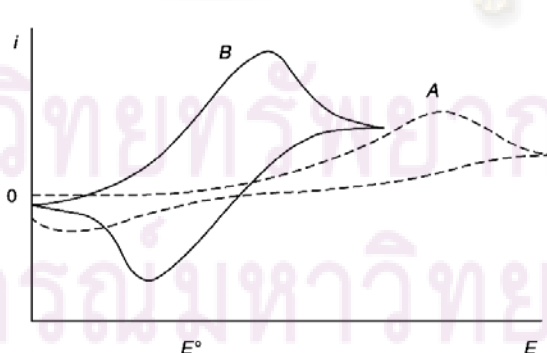
Figure 1.10 Cyclic voltammograms for irreversible (curve A) and quasi-reversible (curve B) redox processes.

For irreversible processes resulting from a slow electron transfer, the reduced and widely separated current peaks are observed shown in Figure 1.10 (curve B). The peak current is still proportional to the concentration, but will be lower in height (about 80% of reversible processes). Figure 1.10 (curve A) represents the cyclic voltammogram of irreversible system.

1.6.2 Electrochemical Cells

The design and construction of a cell must be appropriate with the experimental requirements with respect to shape and size of electrodes, the scale of system (micro or macro), the working temperature and pressure, the stirring requirement and the cell compartments. Glass is widely used for cell material due to the properties of low cost, transparency, chemical inertness and impermeability. Teflon and quartz are provided as an optional material. The cell cover made from any material with chemical inertness is required.

In general experiments, cyclic voltammetric measurements utilize a three-electrode configuration consisting of the working, reference and counter (or auxiliary) electrodes, which are immersed in the sample solution [50]. The reaction occurs at the working electrode and the current passes between this electrode and the counter one. The reference electrode that keeps the potential stable and reproducible can be insulated from the sample solution through an intermediate bridge to reduce contamination from the sample. The auxiliary electrode is typically derived from an inert material such as a platinum wire or graphite rod.

1.6.3 Working Electrodes

The working electrode has played a vital role in the electrochemical measurement, thus its selection has to consider the potential window, the background current, electrical conductivity, surface reproducibility, cost, and toxicity. There are numerous electrodes used in the voltammetric analysis, but the most popular one is a glassy carbon electrode. It provides the excellent properties of electrical conductivity, wide potential window, chemical inertness, reproducible performance, low cost and low background current. The surface pretreatment is usually achieved by polishing with slurry of alumina powder, which keeps the glassy carbon electrodes reactive and

reproducible. After being polished, the electrode should be rinsed with deionized water prior to use.

1.7 Limit of Detection

A limit of detection of an analyte is generally defined as the concentration which gives an instrument signal significantly different from the blank or background signal. This definition of the limit of detection is quite arbitrary and entirely open to an analyst to provide an alternative definition for a particular purpose. However, it is required to provide the definition whenever a detection limit is cited in a paper or report.

This is an alternative definition that defines the detection limit as the analyte concentration giving a signal equal to the blank signal, y_B, plus three standard deviations of the blank, s_B [51].

$$\text{Limit of detection} = y_B + 3s_B \tag{4}$$

According to Eq. (4), the value of a, the calculated intercept of the calibration plot can be used instead of y_B.

1.8 Objective and The Scope of This Research

The aim of this research is to synthesize ligand **L1** containing anthraquinone and imidazolium moieties and study the electrocatalytic properties toward hydrazine oxidation. Firstly, compound **L1** will be synthesized and then modified onto multi-walled carbon nanotubes (MWNTs). The electrocatalytic behavior for the oxidation of hydrazine will be characterized by cyclic voltammetry.

The target molecule **L1** and **L1** modified MWNTs are shown below.
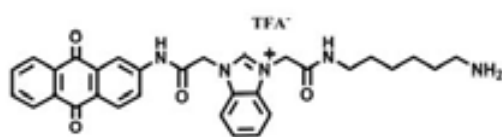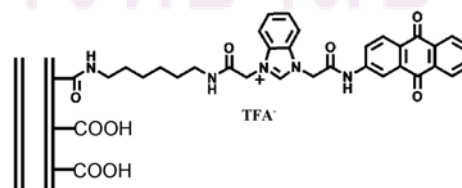
L1   MWNTs

CHAPTER II

EXPERIMENTAL SECTION

2.1 General Procedures

2.1.1 Analytical Instrument

Nuclear magnetic resonance (NMR) spectra were recorded on a Varian 200, 400 and a Bruker DRX 400 MHz nuclear resonance spectrometers. Samples were dissolved in deuterated chloroform and dimethyl sulfoxide. The chemical shift were recorded in part per million (ppm) using residue proton solvents as internal reference. Elemental analysis was carried out on CHNS/O analyzer (Perkin Elmers PE 2400 series II). MALDI-TOF mass spectra were recorded on Bruker Daltonic using doubly recrystallized 2-cyano-4-hydroxy cinnamic acid (CCA) as matrix. IR spectrum of the sample was recorded on a Nicolet Impact 410 FTIR spectrophotometer at room temperature with the potassium bromide (KBr) disk method. The sample was scanned over a range of 500-4000 cm^{-1} at resolution of 16 cm^{-1} and the number of scan was 32. The measurement was controlled by Omnic software. Electrochemical experiments were carried out by μAutolab type III Electrochemical Analyzer with the General Purpose Electrochemical System (GPES) software. A glassy carbon electrode served as working electrode, with an Ag/AgCl (3M KCl) electrode and a platinum wire acting as reference and counter electrodes, respectively. All electrodes were from Metrohm. Data storage and processing were done by a personal computer.

2.1.2 Materials

Unless otherwise specified, the solvent and all materials were reagent grades purchased from Fluka, BDH, Aldrich, Carlo erba, Merck or Lab scan and used without further purification. Commercial grade solvents such as acetone, dichloromethane, hexane, methanol and ethyl acetate were purified by distillation before used. Dimethyl sulfoxide and dichloromethane for setting up the reaction were dried over calcium hydride and freshly distilled under nitrogen atmosphere prior to use. Tetrahydrofuran

was freshly distilled from sodium/benzophenone. Multi-walled carbon nanotubes were obtained from Bayer.

Column chromatography was carried out on silica gel (Kieselgel 60, 0.063-0.200 mm, Merck). Thin layer chromatography (TLC) was performed on silica gel plates (Kieselgel 60, F_{254}, 1 mm). Compounds on TLC plates were detected by the UV-light.

All synthesized compounds were characterized by ^{1}H-NMR spectroscopy, mass spectrometry, IR spectroscopy and elemental analysis. Modified multi-walled carbon nanotubes were all characterized by ^{1}H-NMR spectroscopy, IR spectroscopy and TEM.

2.2 Synthesis of L1

2.2.1 Preparation of 2-(2-chloroacetamido)anthracene-9,10-dione (1)

1
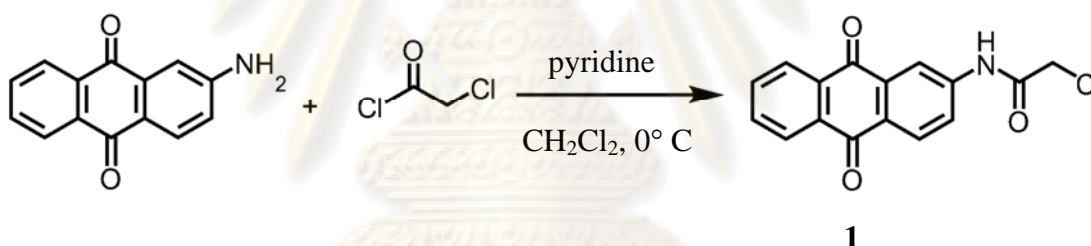
A mixture of 2-aminoanthraquinone (0.992 g, 4.0 mmol) and pyridine (0.43 mL, 5.0 mmol) in dichloromethane (20 mL) was stirred for 10 min under nitrogen atmosphere at room temperature. Chloroacetyl chloride (0.42 mL, 5.0 mmol) in dichloromethane (40 mL) was then added dropwise at ice-cooled condition and kept stirring for 4 h. The reaction mixture was treated with 3M hydrochloric acid (50 mL), extracted with water (2 x 100 mL) and dichloromethane (2 x 100 mL). The organic layer was concentrated on a rotary evaporation and precipitated with hexane to afford a brown solid as the desired product **1** (0.847g, 64%).

Characterization Data for 1

^{1}H-NMR spectrum (400 MHz, CDCl$_3$): δ (ppm)

δ 8.59 (s, 1H, ClCH$_2$CONH), 8.29 (m, 4H, ArH), 8.23 (s, 1H, ArH), 7.81 (m, 2H, ArH), 4.26 (m, 2H, ClCH_2CO).

MALDI-TOF MS C$_{16}$H$_{10}$ClNO$_3$: m/z = 300.57 [**1** + H]$^+$

2.2.2 Preparation of 2-(benzimidazole-1-acetamido)anthracene-9,10-dione (2)
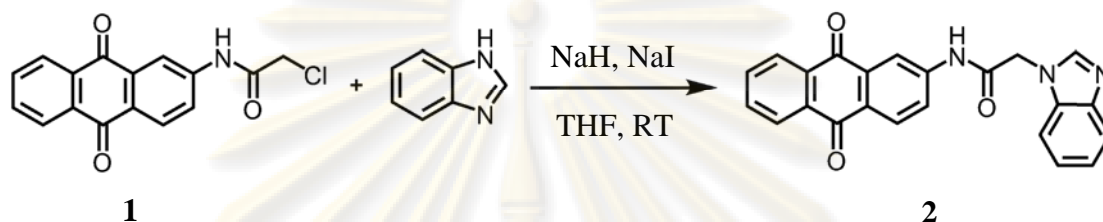
To a stirred dry tetrahydrofuran solution (10 mL) of sodium hydride (0.079 g, 30 mmol), benzimidazole (0.260 g, 2.0 mmol) in tetrahydrofuran (20 mL) was slowly added and kept stirring under nitrogen atmosphere until no bubble gas. A mixture of anthraquinone derivative **1** (0.606 g, 2.0 mmol) and sodium iodide (0.330 g, 2.0 mmol) in tetrahydrofuran was stirred under nitrogen atmosphere for 30 min, subsequently added dropwise into the solution of benzimidazole via cannula.

The resultant mixture was allowed to stir at room temperature overnight. After removal of the solvent by evaporation under vacuum, the residue was further purified by column chromatography in silica gel (dichloromethane/ethyl acetate/methanol, 5:4:1) and recrystallized with THF/DMF (1:1) in warm condition giving a yellow powder as the desired product **2** (0.377 g, 49%).

Characterization Data for 2

^{1}H-NMR spectrum (400 MHz, DMSO): δ (ppm)

δ 11.13 (s, 1H, CONHAr), 8.45 (s, 1H, ArH), 8.26 (s, 1H, ArH), 8.18 (m, 3H, ArH), 8.06 (d, J = 6.8 Hz, 1H, ArH), 7.90 (m, 2H, ArH), 7.68 (d, J = 7.4 Hz, 1H, ArH), 7.57 (d, J = 8.2 Hz, 1H, ArH), 7.23 (m, 2H, ArH), 5.28 (s, 2H, COCH_2N).

MALDI-TOF MS C$_{23}$H$_{15}$N$_3$O$_3$: m/z = 381.69 [**2** + H]$^+$

2.2.3 Preparation of *tert*-butyl 3-aminopropylcarbamate (3)

$$\text{H}_2\text{N-(CH}_2)_6\text{-NH}_2 \;+\; \text{(Boc)}_2\text{O} \;\xrightarrow{\text{CH}_2\text{Cl}_2,\ 0°\text{C}}\; \text{Boc-NH-(CH}_2)_6\text{-NH}_2$$

3
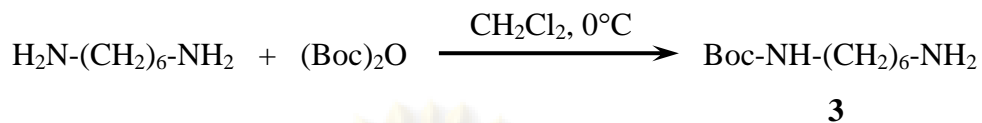
Di-*tert*-butyl dicarbonate (2.032 g, 9.0 mmol) in dichloromethane (50 mL) was slowly added to a dichloromethane solution (90 mL) of 1,6-diaminohexane (10.782 g, 93 mmol) with stirring and cooling in an ice bath during 3 h under nitrogen atmosphere. The mixture was stirred further for 16 h at room temperature and then extracted with water (8 x 100 mL). The organic phase was dried over anhydrous sodium sulfate and evaporated to dryness in vacuum. The desired product **3** (1.627 g, 81%) was obtained as colorless oil used for the further step without purification.

Characterization Data for 3

^{1}H-NMR spectrum (400 MHz, CDCl$_3$): δ (ppm)
δ 4.63 (s, 1H, CON*H*CH$_2$), 3.05 (d, J = 6.06 Hz, 2H, (CH$_2$)$_5$C*H$_2$*NHCO), 2.62 (t, J = 7.07 Hz, 2H, NH$_2$C*H$_2$*(CH2)$_5$NHCO), 1.53 (s, 2H, N*H$_2$*(CH$_2$)$_6$), 1.40 (s, 9H, C(C*H$_3$*)$_3$), 1.28 (m, 8H, NH$_2$CH$_2$(C*H$_2$*)$_4$CH$_2$N).

2.2.4 Preparation of *tert*-butyl 3-(2-chloroacetamido)propylcarbamate (4)

$$\text{Boc-NH-(CH}_2)_6\text{-NH}_2 + \text{ClCOCH}_2\text{Cl} \;\xrightarrow[\text{CH}_2\text{Cl}_2,\ 0°\text{C}]{\text{pyridine}}\; \text{ClCH}_2\text{CONH-(CH}_2)_6\text{-NH-Boc}$$

3   **4**
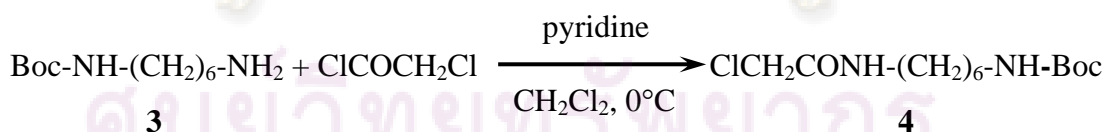
A dichloromethane solution (60 mL) of Boc-amine **3** (1.627 g, 8.0 mmol) and pyridine (0.73 mL, 9.0 mmol) was stirred under nitrogen atmosphere for 10 min at room temperature. Chloroacetyl chloride (0.72 mL, 9.0 mmol) in dichloromethane (80 mL) was then added dropwise with cooling in an ice bath under nitrogen atmosphere. The reaction mixture was further kept stirring for 4 h at room temperature. After the reaction completed, 3M hydrochloric acid (100 mL) was added and stirred for 30 min.

The resultant mixture was then extracted with water (3 x 100 mL) and dichloromethane (3 x 100 mL). The organic layer was dried over anhydrous sodium sulfate and evaporated under vacuum affording a white solid as the desired product **4** (1.523 g, 69%).

Characterization Data for 4

^{1}H-NMR spectrum (400 MHz, CDCl$_3$): δ (ppm)

δ 6.58 (s, 1H, CON*H*C), 4.49 (s, 1H, OCON*H*C), 3.98 (s, 2H, ClC*H$_2$*CO), 3.23 (m, 2H, OCONHC*H$_2$*CH$_2$), 3.03 (m, 2H, CONHC*H$_2$*CH$_2$), 1.37 (s, 9H, C(C*H$_3$*)$_3$), 1.28 (m, 8H, NCH$_2$(C*H$_2$*)$_4$CH$_2$N).

MALDI-TOF MS C$_{13}$H$_{25}$ClN$_2$O$_3$: m/z = 293.63 [**4** + H]$^+$

2.2.5 Preparation of Boc-Ligand Containing Anthraquinone and Imidazolium Moieties (5)
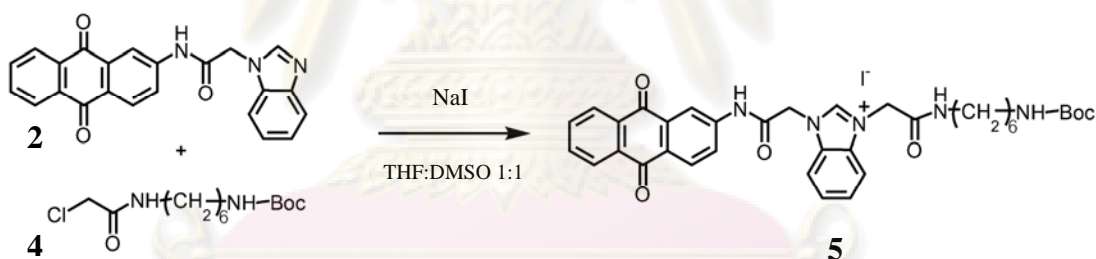
A tetrahydrofuran solution (10 mL) of compound **4** (0.161 g, 0.5 mmol) and sodium iodide (0.082 g, 0.5 mmol) was kept stirring under nitrogen atmosphere for 30 min. A THF/DMSO (1:1) solution (10 mL) of anthraquinone derivative **2** (0.191 g, 0.5 mmol) was allowed to stir under nitrogen atmosphere, and heated until dissolved. Two portions were gradually mixed together via cannula and stirred at room temperature overnight. The reaction mixture was evaporated under reduce pressure providing dimethyl sulfoxide residue. To afford the desired product, precipitation was performed by water, dichloromethane and methanol yielding an orange solid (0.084 g, 26%).

Characterization Data for 5

^{1}H-NMR spectrum (400 MHz, DMSO): δ (ppm)

δ 11.46 (s, 1H, ArN*H*CO), 9.79 (s, 1H, Ar*H*), 8.59 (s, 1H, CON*H*C), 8.51 (s, 1H, Ar*H*), 8.19 (m, 3H, Ar*H*), 8.07 (m, 2H, Ar*H*), 7.92 (m, 3H, Ar*H*), 7.70 (m, 2H, Ar*H*), 6.77 (s, 1H, CN*H*COO), 5.69 (s, 2H, NC*H₂*CO), 5.38 (s, 2H, NC*H₂*CO), 3.12 (m, 2H, (CH₂)₅C*H₂*NHCOOC(CH₃)₃) , 2.87 (m, 2H, CONHC*H₂*(CH₂)₅NHCOOC(CH₃)₃), 1.43 (m, 4H, NCH₂C*H₂*CH₂CH₂C*H₂*CH₂N), 1.35 (s, 9H, COOC(C*H₃*)₃), 1.25 (m, 4H, NCH₂CH₂C*H₂*C*H₂*CH₂CH₂N).

MALDI-TOF MS C₃₆H₄₀N₅O₆: m/z = 637.95 [**5**]⁺

2.2.6 Preparation of ligand L1 Containing Anthraquinone and Imidazolium Moieties

A dichloromethane solution (4 mL) of compound **5** (0.458 g, 0.7 mmol) and trifluoroacetic acid (1 mL, 13 mmol) was stirred under nitrogen atmosphere at room temperature for 1 h. After the reaction completed, solvent was removed to dryness. The resultant product was washed with dichloromethane and methanol several times to remove the excess trifluoroacetic acid, providing a brown solid as the desired product (0.418 g, 90%).

Characterization Data for L1

^{1}H-NMR spectrum (400 MHz, DMSO): δ (ppm)

δ 11.62 (s, 1H, ArN*H*CO), 9.83 (s, 1H, Ar*H*), 8.73 (s, 1H, CON*H*C), 8.53 (s, 1H, Ar*H*), 8.19 (m, 3H, Ar*H*), 8.09 (m, 2H, Ar*H*), 7.93 (m, 3H, Ar*H*), 7.70 (m, 2H, Ar*H*), 5.72 (s, 2H, NC*H₂*CO), 5.40 (s, 2H, NC*H₂*CO), 3.14 (m, 2H, CONHC*H₂*(CH₂)₅NH₂) , 2.74 (m, 2H, CONH(CH₂)₅C*H₂*NH₂, 1.51 (m, 2H, CONHCH₂C*H₂*(CH₂)₄NH₂), 1.45 (m, 2H, CONH(CH₂)₄C*H₂*CH₂NH₂), 1.29 (m, 4H, CONH(CH₂)₂C*H₂*C*H₂*(CH₂)₂NH₂).

MALDI-TOF MS C₃₁H₃₂N₅O₄: m/z = 537.87 [**L1**]⁺

2.3 Synthesis of L2 by Solid Phase Method

In order to compare anion recognition with **L1**, ligand **L2** providing more rigid framework was synthesized. From ^{1}H-NMR spectrum, we found the characteristic peaks of **L2**, but it could not be purified by either column chromatography or crystallization. Therefore, we tried to synthesize **L2** by solid phase synthesis, schematically illustrated by the following procedure. However, we could not afford ligand **L2** because of low solubility of compound **10** in any solvents. The structure of **L2** was shown below.

L2

2.3.1 Synthetic Pathway of L2

Merrifield resin   4-hydroxybenzyl alcohol   K$_2$CO$_3$/KI   DMF, over night   **6**

6

+

4-nitrophenyl chloroformate   pyridine, CH$_2$Cl$_2$, 5-6 h   **7**

7   H$_2$N(CH$_2$)$_6$NH$_2$ (excess)   **8**

8   DIC, CH$_2$Cl$_2$ + DMF   **9**

9

10

NaI, DMF

11

TFA, CH₂Cl₂
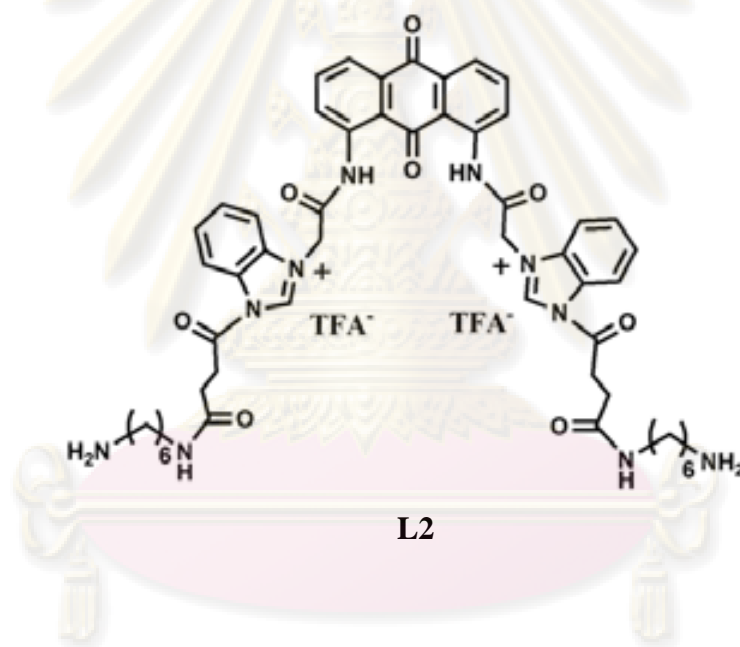
L2
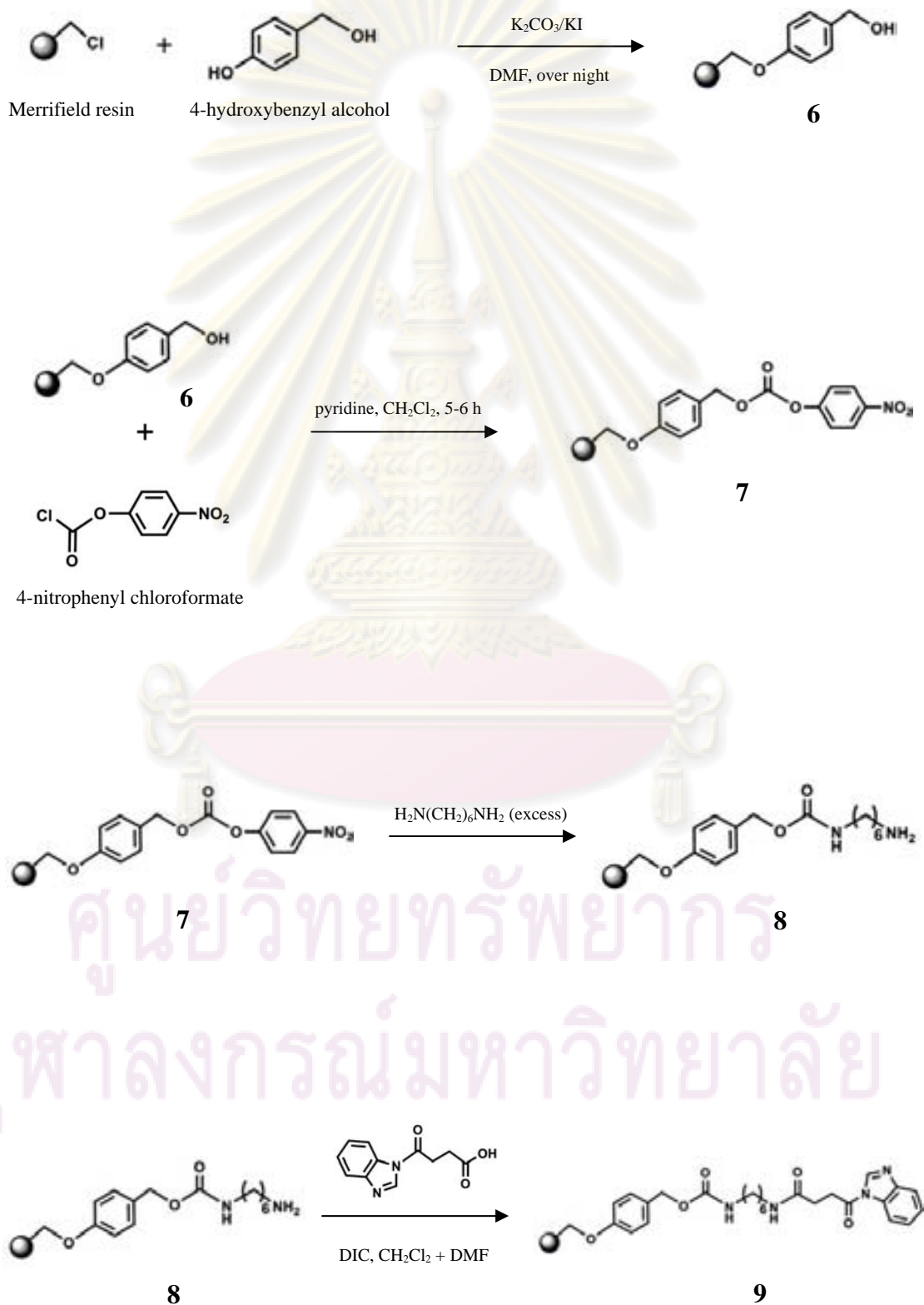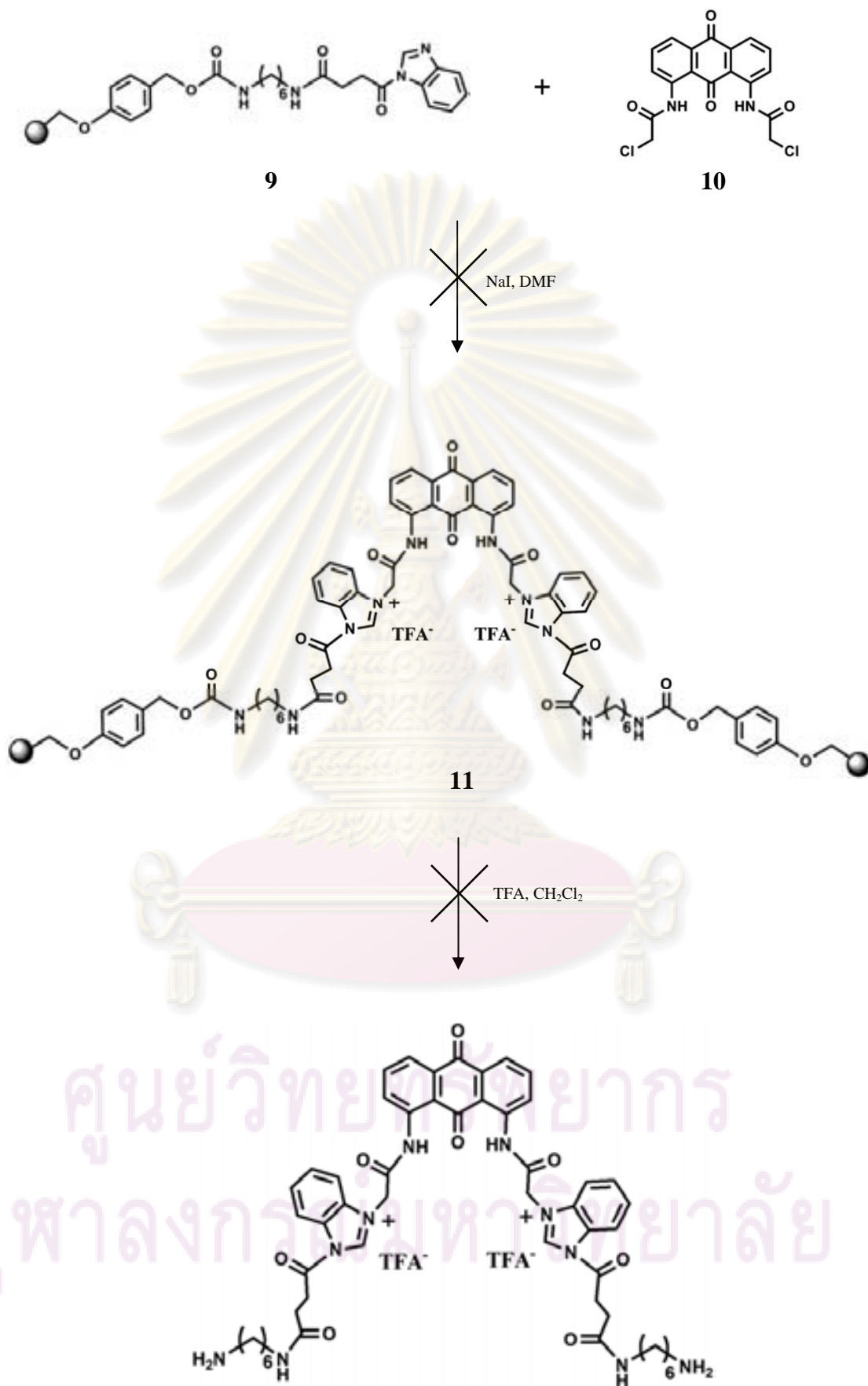
2.4 Modification of Multi-Walled Carbon Nanotubes with L1

2.4.1 Oxidation of Multi-Walled Carbon Nanotubes

Raw multi-walled carbon nanotubes (5.000 g) were suspended in 100 mL of a 3:1 mixture of concentrated sulfuric and nitric acid. The mixture was stirred at 40°C for 5 h. After completion, the resultant mixture was cooled down to room temperature, diluted with 500 mL of cold distilled water and then filtered through a 0.65 µm pore size Durapore DVPP filter paper. The filtrate was washed with distilled water until no residual acid was present. The oxidized MWNTs were then dried in an oven at 80°C for 4 h and used without any further pretreatment.

2.4.2 Chlorination and Functionalization of MWNTs with L1

The carboxylic acid functionalized MWNTs (0.150 g) were dissolved in DMF (5 mL) and ultrasonicated for 1 h to achieve a homogeneous solution. Oxalyl chloride (0.3 mL, 4.0 mmol) was added into the mixture and stirred under nitrogen atmosphere for 30 min providing the chlorinated MWNTs. The reaction mixture was washed with CH_2Cl_2 (30 mL) to remove any residual oxalyl chloride. The ligand **L1** (0.150 g, 0.2 mmol) and pyridine (0.05 mL, 0.6 mmol) in DMF (5 mL) were allowed to stir under nitrogen atmosphere for 30 min to deprotonate proton of NH_2 group and sequentially reacted with the chlorinated MWNTs. After the reaction completed, it was kept stirring overnight. The solid was collected by filtration through the 0.65 µm pore size Durapore DVPP filter paper and washed with dichloromethane and methanol to remove the excess reactants. Modified MWNTs were dried at 40°C for 24 h.

2.5 Electrochemical Studies of Ligand L1 by Cyclic Voltammetry

2.5.1 Preparation of MWNTs/Nafion Coated Glassy Carbon Electrodes

Prior to modification, a bare glassy carbon electrode was polished with 1.0 and 0.3 µm alumina slurries to obtain a mirror-like surface, and ultrasonicated in 1M sulfuric acid solution, distilled water, and methanol, sequentially.

A 1.0 wt% Nafion solution was prepared by diluting the 5.0 wt% Nafion solution with ethanol. One milligram of MWNTs was added into 1 mL of 1.0 wt% Nafion solution and ultrasonicated for 1 h to form a homogeneous Nafion/MWNTs suspension. The modification of bare glassy carbon electrode was as the following. A 5 µL aliquot of the resultant MWNTs/Nafion suspension was dispersed onto the electrode surface and allowed to evaporate ethanol at room temperature in air providing the MWNTs/Nafion coated glassy carbon electrode.

2.5.2 Electrocatalytic Activities of Modified Electrodes toward Hydrazine and $Na_2S_2O_3$

Electrochemical experiments were carried out in pH 7 buffer solution supporting electrolyte medium. Distilled water was used to prepare all solutions, and buffer solutions (0.1 molL^{-1}) were prepared from HEPES (4-(2-hydroxyethyl)-1-piperazineethanesulfonic acid) and sodium chloride (NaCl). The electrochemical cells consisted of a three-electrode arrangement with the Ag/AgCl (3M KCl) as reference electrode, the Pt wire as counter electrode and the glassy carbon (modified with MWNTs-COOH or MWNTs/**L1**) as working electrode. All three electrodes were inserted into a 10 mL electrochemical cell through holes in its Teflon cover. A stock solution of 0.5 M hydrazine or $Na_2S_2O_3$ in buffer solution (pH 7) was prepared by a 5 mL volumetric flask.

Cyclic voltammetric titration was investigated by continuous potential cycling from 0.0 to 0.5 V at scan rate 100 mVs^{-1}. All electrochemical measurements were performed at room temperature. The solution of 0.5 M hydrazine or $Na_2S_2O_3$ was added into 5.0 mL of buffer solution in the cell by a micro-syringe. Prior to the experiments, the solution was de-aerated with nitrogen for 5 min, and stirred for 10 s after each addition of hydrazine.

Table 2.1 The concentration of hydrazine solution used in electrochemical studies of ligand **L1**

Point	[Hydrazine] μM	V of Hydrazine (μL)	V total (μL)
1	0.1	1	1
2	0.2	1	2
3	0.3	1	3
4	0.4	1	4
5	0.5	1	5
6	0.6	1	6
7	0.7	1	7
8	0.8	1	8
9	0.9	1	9
10	1.0	1	10
11	1.2	2	12
12	1.4	2	14
13	1.6	2	16
14	1.8	2	18
15	2.0	2	20
16	2.5	5	25
17	3.0	5	30
18	3.5	5	35
19	4.0	5	40
20	4.5	5	45
21	5.0	5	50
22	6.0	10	60
23	7.0	10	70
24	8.0	10	80
25	9.0	10	90
26	10.0	10	100

Table 2.2 The concentration of $Na_2S_2O_3$ solution used in electrochemical studies of ligand **L1**

Point	[$Na_2S_2O_3$] μM	V of $Na_2S_2O_3$ (μL)	V total (μL)
1	0.1	1	1
2	0.2	1	2
3	0.3	1	3
4	0.4	1	4
5	0.5	1	5
6	0.6	1	6
7	0.7	1	7
8	0.8	1	8
9	0.9	1	9
10	1.0	1	10
11	1.2	2	12
12	1.4	2	14
13	1.6	2	16
14	1.8	2	18
15	2.0	2	20
16	2.5	5	25
17	3.0	5	30
18	3.5	5	35
19	4.0	5	40
20	4.5	5	45
21	5.0	5	50
22	6.0	10	60
23	7.0	10	70
24	8.0	10	80
25	9.0	10	90
26	10.0	10	100

CHAPTER III

RESULTS AND DISCUSSION

3.1 Design Concept

Selective anion receptors based on imidazolium moiety have attracted tremendous interest from scientists due to a strong interaction with anions through (C-H)$^+$ $\cdots$X$^-$ charged hydrogen bonding. It was presented that imidazolium derivatives utilized strong hydrogen bonding between imidazolium group and anions such as halide ions and $H_2PO_4^-$ etc [52-53]. Consequently, the combination of this particular type of interaction and any of potential signaling units can generate powerful anion sensors.

Among various signaling units, the most important one is an electrochemical signal. Anthraquinone derivatives providing both electrochemical and chromogenic signals have been typically studied the properties toward anion recognition. The significant changes of electrical behavior upon the complexation with anions can be investigated by electrical methods. Thus, the inclusion of the anthraquinone group in the receptors enables them to be used as electrochemical anion receptors.

Carbon nanotubes with fascinating mechanical, electrical and chemical properties have been widely applied in the field of nanotechnology, material science, catalysis and nanobiotechnology etc. The promising electrical conductivity of the nanotubes leads to the application of electrical devices. It was suggested that CNTs derivatives have been prepared and utilized as electrodes in electrochemical sensors and electrocatalytic activities. Low solubility of CNTs limits them to spread out a wide range of applications; however, the chemical modification via both covalent and non-covalent attachments allows the change of soluble property.

According to aforementioned reasons, our researches have focused on the synthesis of ligand consisting of anthraquinone and imidazolium moieties and modification onto the nanotube surface with the covalent attachment to afford an ideal miniaturized sensor for anions. We placed anthraquinone part for an electrochemical signaling unit, amide and imidazolium groups for anion binding. It was expected that

the chemical functionalization of nanotubes would allow them to be used as electrodes for electrochemical analysis, as well as improving their solubility.

Consequently, we synthesized the ligand **L1** and immobilized onto multi-walled carbon nanotube surface. The modified MWNTs/ligand electrodes were prepared. The electrochemical behavior toward anions and electrocatalytic properties were carried out by cyclic voltammetric studies. The synthetic pathway of ligand **L1** was depicted in Scheme 3.1.
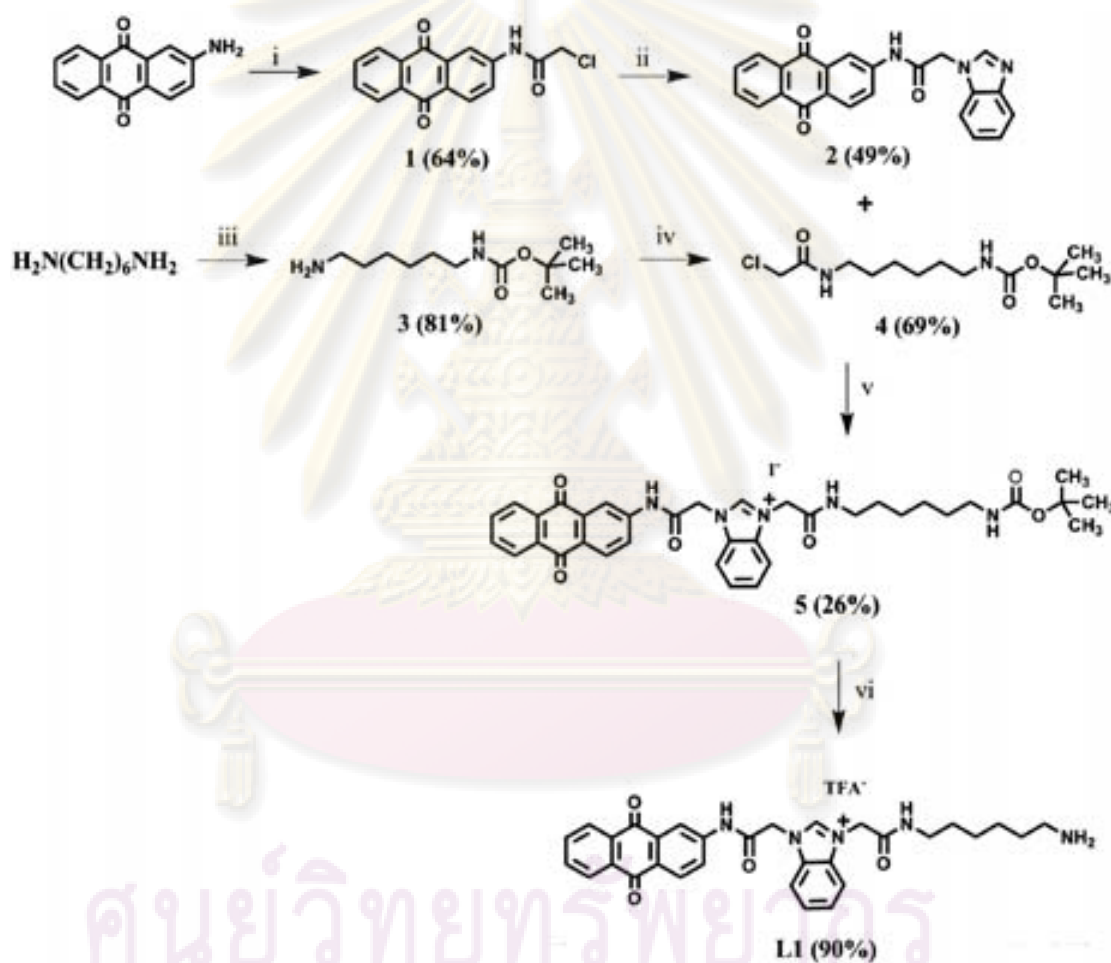
Scheme 3.1 Synthetic pathway of anthraquinone derivative **L1**.

(i) chloroacetyl chloride, pyridine, CH_2Cl_2; (ii) benzimidazole, NaI, NaH, THF; (iii) di-*tert*-butyl dicarbonate, CH_2Cl_2; (iv) chloroacetyl chloride, pyridine, CH_2Cl_2; (v) NaI, THF/DMSO (1:1); (vi) TFA,CH_2Cl_2

3.2 Synthesis and Characterization of Anthraquinone Derivative Containing Imidazolium Moiety (L1)

The synthesis of ligand **L1** was started from chlorination of 2-aminoanthraquinone with chloroacetyl chloride using pyridine as base. The mixture was stirred under nitrogen atmosphere for 4 h and also cooled down to 0°C while adding chloroacetyl chloride to avoid a vigorous reaction. The reaction was then treated with 3M hydrochloric acid for removing any residual pyridine, extracted with water and dichloromethane and precipitated with hexane providing chloroacetamido anthraquinone **1** as a brown solid in 64% yield. The ^{1}H-NMR spectrum showed the singlet signal of N*H* amide group at 8.59 ppm, the singlet assignment of ClC*H$_2$*CO protons at 4.26 ppm and the signal of aromatic protons in a range of 8.34-7.80 ppm. Moreover, the characterization of mass spectrometry showed the strong peak at m/z 300.57 corresponding to chloroacetamido anthraquinone structure.

Chloroacetamido anthraquinone **1** was reacted with benzimidazole in the presence of sodium hydride as base and sodium iodide as catalyst in tetrahydrofuran. After the reaction completed, the solvent was removed by evaporation under vacuum. Because of low solubility of the product, it was mixed with small amount of silica gel and prepared a column in the solid phase. Column chromatography was carried out using dichloromethane/ethyl acetate/methanol (5:4:1) as eluent. The product was also recrystallized with the warm THF/DMF (1:1) mixture to get benzimidazole anthraquinone **2** as a yellow solid in 49% yield. ^{1}H-NMR data of compound **2** exhibited the significant downfield shift of the N*H* signal of amide group (from 8.59 to 11.13 ppm), the range of aromatic protons and the singlet of ClC*H$_2$*CO protons (from 4.26 to 5.28 ppm). All mentioned protons were influenced from benzimidazole moiety. The characteristic of compound **2** also included the singlet signal of NC*H*N proton at 8.26 ppm. Besides the ^{1}H-NMR results, the intense peak of mass spectrum at m/z 381.69 is a good agreement with the structure of **2**.

Protected amine **3** was prepared by the reaction between 1,6-diaminohexane and di-*tert*-butyl dicarbonate. The reaction was stirred and kept in an ice bath while slowly adding 0.1 equiv. of (Boc)$_2$O to prevent the attachment of protecting group at both sides. During the addition of di-*tert*-butyl dicarbonate, white precipitate was formed indicating that the reaction has occurred. After extracted with water, the

desired product was obtained as colorless oil in 81% yield. The singlet signal of N*H* amide proton appeared in the ^{1}H-NMR spectrum at 4.63 ppm. The signals of aliphatic protons in a range of 3.06-1.27 ppm and the singlet peak of (Boc)$_2$O protons at 1.40 ppm were observed in the spectrum. The appearance of the singlet assignment of amine group also confirmed the accomplishment of the desired product **3**.

Transformation of Boc-primary amine to Boc-chlorinated amine **4** was performed in the same condition as the chlorination of 2-aminoanthraquinone already mentioned above. ^{1}H-NMR spectrum showed two singlet signals of amide protons at 6.58 and 4.49 ppm and the singlet peak of COC*H*$_2$Cl at 3.98 ppm. Furthermore, a range of aliphatic protons slightly shifted to downfield that received an influence from electron withdrawing effect of the carbonyl group. All results were also confirmed by mass spectroscopy showing a peak at m/z 293.63.

We took attempts to find out the suitable solvent system for the reaction of anthraquinone derivative **2** and alkyl chain **4** due to poor solubility of compound **2**. Finally, we found a proper condition using the mixture of THF and DMSO (1:1). However, the desired compound was obtained only 26% yield. Anthraquinone portion dissolved in THF/DMSO mixture was heated to improve the solubility giving yellow solution. In THF solvent, Boc-chlorinated amine was stirred with sodium iodide for 30 min for anion exchanged compound to provide colorless solution of iodide compound. During an exchange of leaving group, we found white precipitate of sodium chloride. Then, THF solution was added dropwise into THF/DMSO mixture via cannula. The color of reaction changed to orange. All steps for this compound were kept stirring under nitrogen atmosphere since iodide was very sensitive to air. After removed solvent by evaporation, residue of DMSO was left. Boc-ligand **5** was purified by precipitation with water, dichloromethane and methanol affording an orange solid in 26% yield. From the ^{1}H-NMR spectrum, we found the characteristic peak of three N*H* amide groups at 11.46, 8.59 and 6.77 ppm, ClC*H*$_2$CO protons at 5.69 and 5.38 ppm. All aromatic signals and singlet of ClC*H*$_2$CO protons shifted considerably to downfield due to positive charge of imidazolium salt. An intense peak at m/z 637.95 of mass spectrum also supported the structure of compound **5**.

Finally, ligand **L1** was achieved through the following procedure. Dichloromethane solution of compound **5** and trifluoroacetic acid was stirred under nitrogen atmosphere for 1 h in order to remove the protecting group. After completion, the reaction was dried by evaporation to provide a dark brown solid of

the desired compound with the remaining TFA. This precipitate was washed with methanol and dichloromethane to get rid of any residual TFA yielding **L1** as a brown solid in 90% yield.

The ^{1}H-NMR pattern of **L1** shows similarity to that of compound **5** but the signals of Boc group were not found in ^{1}H-NMR spectrum of **L1**. This result was expected that the de-Boc process was accomplished. Moreover, the characterization by MALDI-TOF mass spectroscopy showing at Figure 3.2 can confirm the existence of ligand **L1**. At this stage, the protecting group was removed in order to regain amine group for the further reaction.
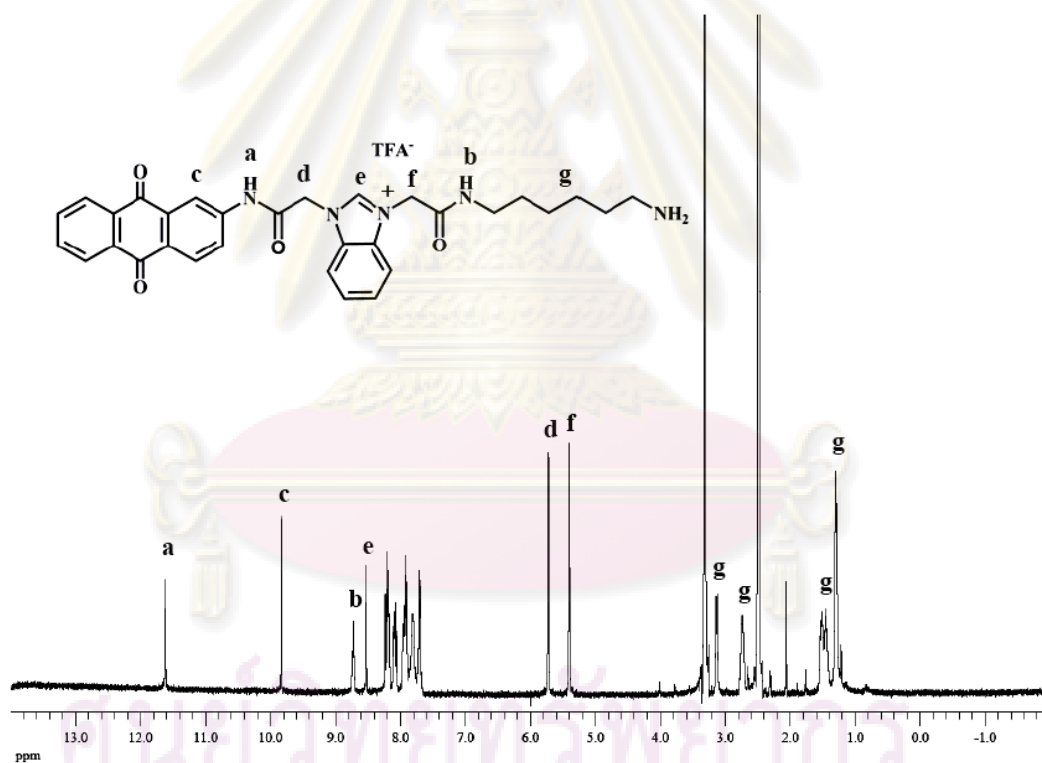
Figure 3.1 The ^{1}H-NMR spectrum of ligand **L1** consisting of anthraquinone derivative and imidazolium salt in DMSO-d6.
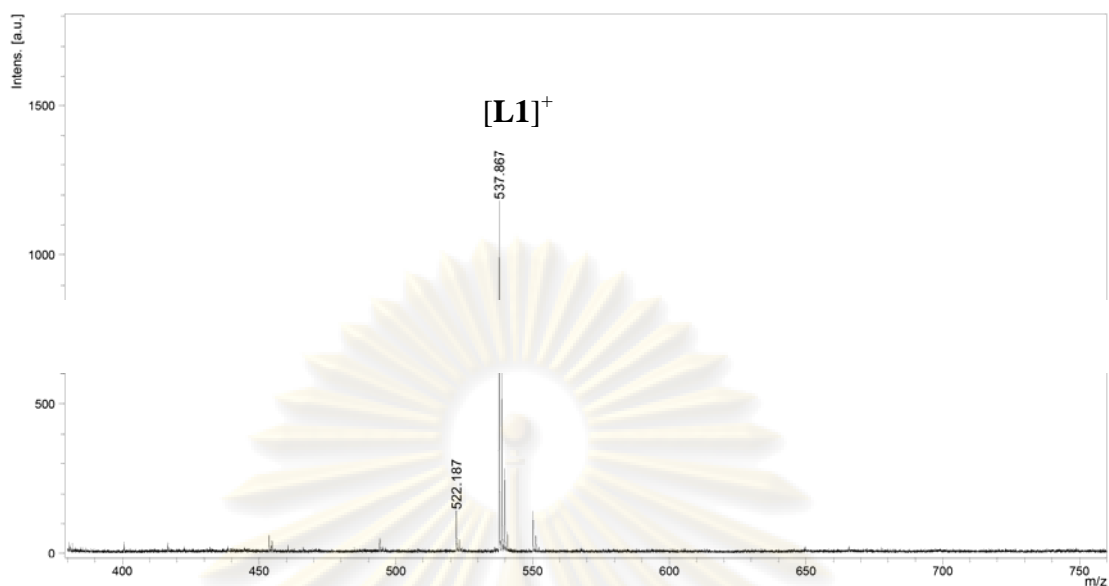
**Figure 3.2** MALDI-TOF mass spectrum of **L1**.

## 3.3 Modification and Characterization of Multi-Walled Carbon Nanotubes

The main objective of this research is to apply the synthesized ligand as an electrochemical device. Therefore, we attempted to construct the covalent bond between ligand **L1** and carbon nanotubes. Methods for the functionalization of MWNTs with anthraquinone derivative containing imidazolium salt were depicted in Scheme 3.2. The pristine MWNTs were firstly treated with a 3:1 mixture of concentrated sulfuric and nitric acid providing carboxylated functionalized MWNTs [54]. Oxidation of the CNTs not only remove the remaining metallic catalysts but also shorten the nanotubes length by forming carboxylic groups at the defects of the graphene layer. Carboxylation was a proper method for this work because it could be covalently bonded to form amide or ester linkages. Obviously, after the acid treatment of the nanotubes, MWNTs-COOH were suspended homogeneously in DMF and other organic solvents, but it settled down after few hours. Afterward, oxidized MWNTs were transformed into chlorinated functionalized nanotubes by the reaction with oxalyl chloride in DMF, and successively functionalized with ligand **L1** forming the amide bonds. After filtration and drying at 40°C for 24 h, modified CNTs were characterized by ^{1}H-NMR (Figure 3.3), IR (Figure 3.4) and TEM (Figure 3.5) techniques prior to study on the electrochemical properties by cyclic voltammetry.
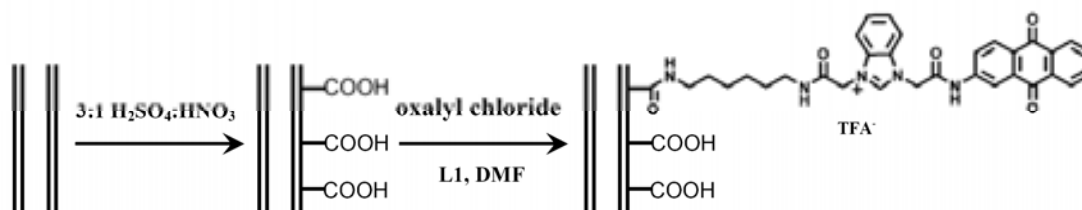
Scheme 3.2 Functionalization of MWNTs with ligand **L1** based on anthraquinone derivative and imidazolium salt.

3.3.1 Characterization of Ligand L1 Modified MWNTs by ^{1}H-NMR
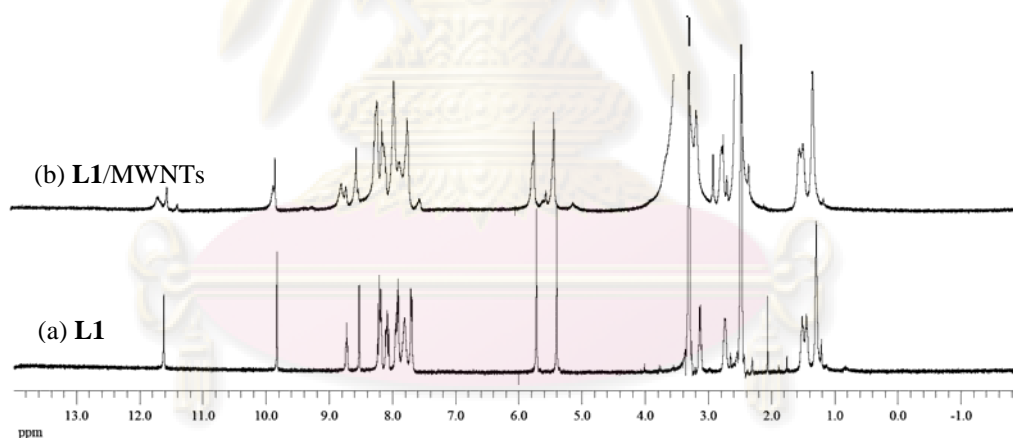
Figure 3.3 The ^{1}H-NMR spectra of ligand **L1** (a) and **L1** modified MWNTs (b) in DMSO-d6.

The ^{1}H-NMR spectrum of **L1** modified MWNTs were recorded in deuterated DMSO. Since the modified nanotubes could not be dissolved in DMSO very well, the broad signals were observed in the spectrum. Nevertheless, it clearly showed the signals in aromatic region correspond to anthraquinone and imidazole moieties, and the proton assignments of the alkyl amine linker.

3.3.2 Characterization of Ligand L1 Modified MWNTs by FT-IR
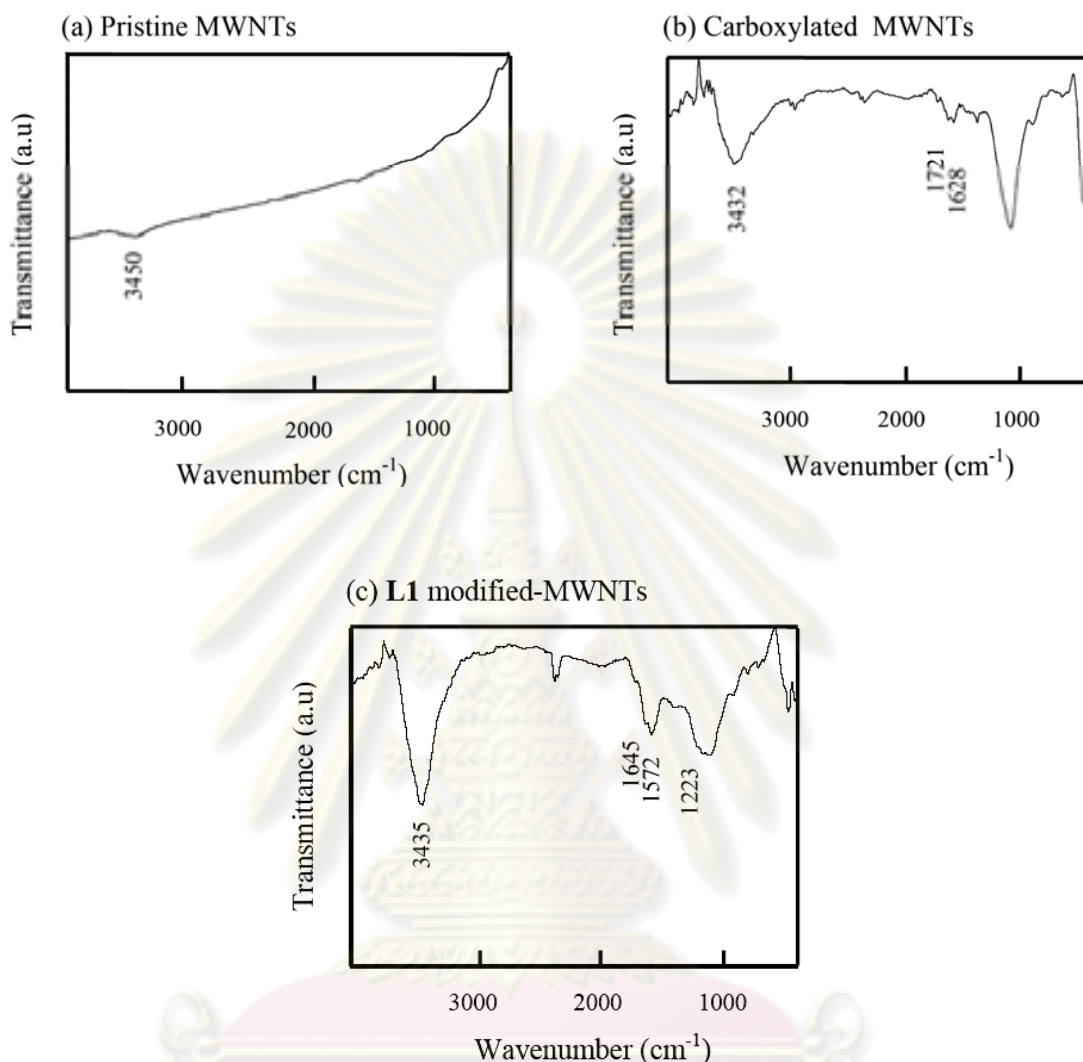
Figure 3.4 FT-IR spectra of MWNTs samples (a) Pristine, (b) carboxylated, and (c) **L1** modified MWNTs.

The FT-IR spectrum of pristine MWNTs (Figure 3.4a) appeared weak broad band at $\sim$3450 cm^{-1} which was attributed to OH group on the surface of nanotubes and possibly occurred from either atmosphere moisture or oxidation during the purification process. In the spectrum of the acid treated MWNTs (Figure 3.4b), the peak at $\sim$3432 cm^{-1} was assigned to OH group of carboxylic and the band of carboxylic carbonyl (C=O) stretching was shown at $\sim$1721 cm^{-1}. The spectrum of **L1** modified MWNTs (Figure 3.4c) exhibited C=O stretching of amide group at lower frequency (1645 cm^{-1}), and the new peaks at 1572 as well as 1223 cm^{-1} correspond to

N-H in plane and C-N stretch respectively. The appearance of C=O amide stretching also verified the attachment of ligand **L1** to the nanotube surface.

3.3.3 Characterization of Pristine and Acid-Treated MWNTs by TEM
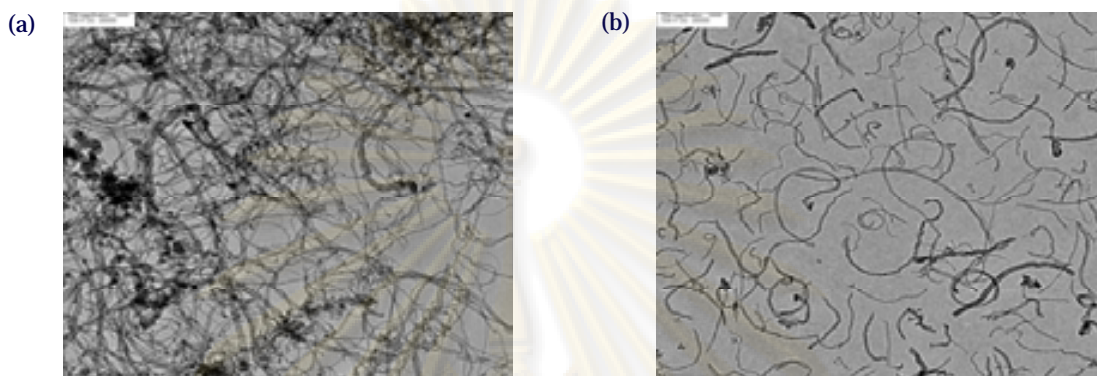
Figure 3.5 TEM images of (a) pristine and (b) carboxylated MWNTs.

TEM images of MWNTs were shown in Figure 3.5. Pristine MWNTs (Figure 3.5a) were typically aggregated in bundles and revealed black spots of metallic (iron) nanoparticles. However, TEM image of the acid treated nanotubes (Figure 3.5b) showed less bundles than what were found for pristine CNTs. This observation also confirmed the chemical oxidation on the nanotubes surface with 3:1 H_2SO_4/HNO_3 mixture, which was able to cut the long ropes of carbon nanotubes into short, open-ended pipes.

3.4 Electrochemical Studies of Ligand L1 by Cyclic Voltammetry

      3.4.1 Cyclic Voltammetric Response of L1/MWNTs Modified GC Electrodes
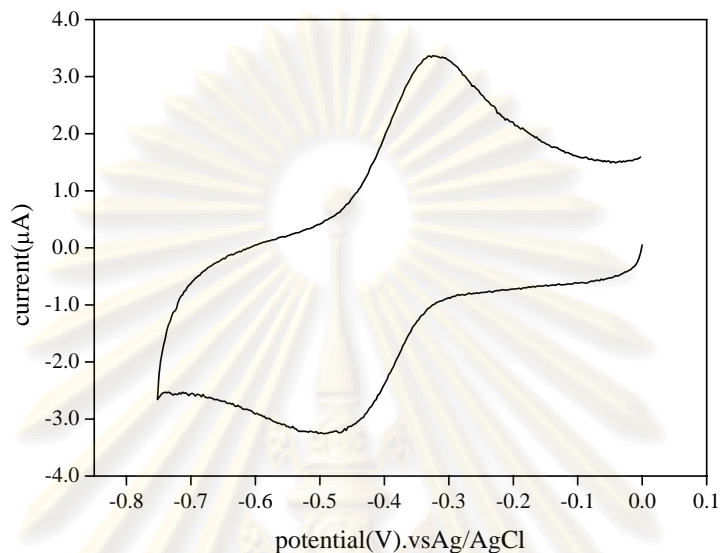
**Figure 3.6** Cyclic voltammogram of **L1**/MWNTs modified glassy carbon electrode in pH 7 buffer solution (HEPES + NaClO$_4$), scan rate 100 mVs^{-1}.

      After the functionalization of MWNTs with ligand **L1**, the coated glassy carbon electrodes were prepared. The modified electrode was immersed in the buffer solution and the potential cycling was carried out between 0.0 and -0.75 V (vs Ag/AgCl (sat), 3 M KCl). The cyclic voltammetric response (Figure 3.6) recorded at 100 mVs^{-1} showed a pair of well-defined redox waves due to the Q/QH$_2$ couple of attached anthraquinones [55]. From the experimental result, it indicated that the synthesized ligand was properly immobilized on the nanotube surface.
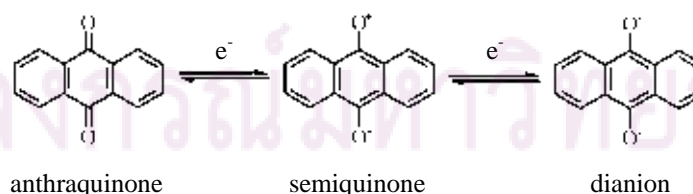

Figure 3.7 The redox reaction of anthraquinone-hydroquinone system.

As mentioned in chapter I, the redox reaction of anthraquinone involves the stepwise transfer of two-electron electrochemical reductions. Anthraquinone is firstly reduced to semiquinone and dianion is the product of the second reduction, shown in Figure 3.7.

3.4.2 Cyclic Voltammetric Response of L1/MWNTs Modified GC Electrodes toward Anions

Based on $(C-H)^+ \cdots X^-$ hydrogen bonding of imidazolium group, we attempted to study the binding interaction of ligand **L1** with anions including F^-, Cl^-, Br^-, I^- and $H_2PO_4^-$. However, anion recognition was not observed. This could be attributed to π-π stacking interaction between **L1** and the graphitic sidewalls of nanotubes that gave rise to the inappropriate structure of immobilized **L1** for anion binding.

3.4.2.1 Cyclic Voltammetric Response of L1/MWNTs Modified GC Electrodes toward F⁻
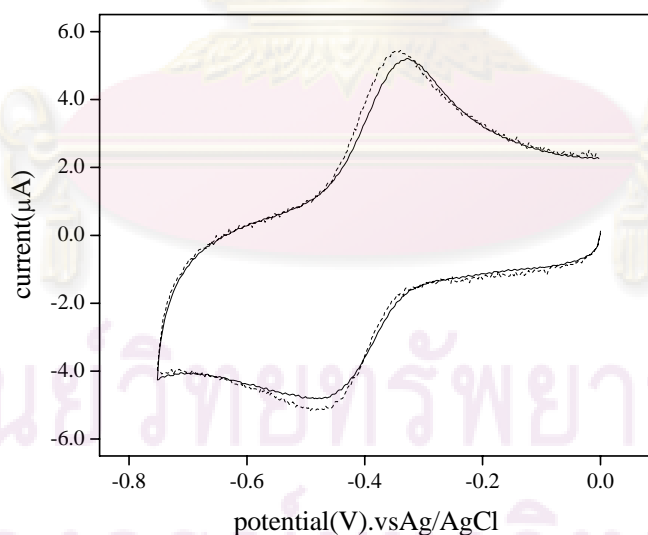
Figure 3.8 Cyclic voltammograms of **L1**/MWNTs modified glassy carbon electrode in pH 7 buffer solution (HEPES + NaClO$_4$) in the absence (solid line) and presence (dash line) of F$^-$ 1.0 mM, scan rate 100 mVs^{-1}.

After adding an excess F⁻, the cyclic voltammogram showed insignificant changes of both anodic and cathodic waves suggesting that there was no interaction between F⁻ and ligand **L1** modified MWNTs.

3.4.2.2 Cyclic Voltammetric Response of L1/MWNTs Modified GC Electrodes toward Cl⁻

Figure 3.9 Cyclic voltammograms of **L1**/MWNTs modified glassy carbon electrode in pH 7 buffer solution (HEPES + NaClO$_4$) in the absence (solid line) and presence (dash line) of Cl⁻ 1.0 mM, scan rate 100 mVs^{-1}.

After adding an excess Cl⁻, the cyclic voltammogram showed insignificant changes of both anodic and cathodic waves suggesting that there was no interaction between Cl⁻ and ligand **L1** modified MWNTs.
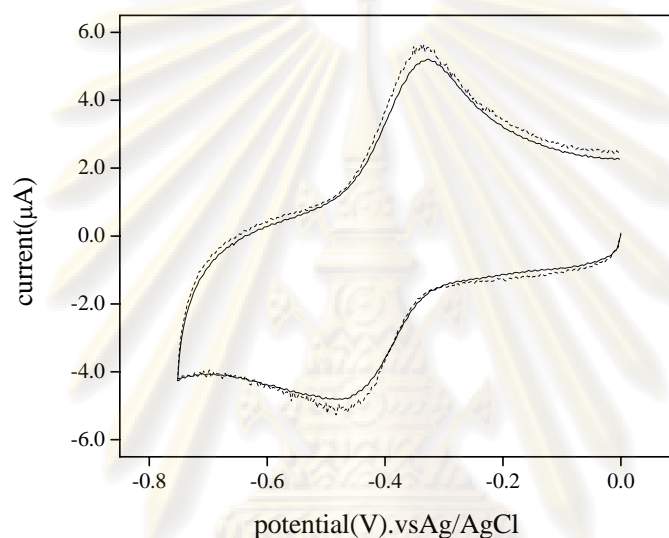
3.4.2.3 Cyclic Voltammetric Response of L1/MWNTs Modified GC Electrodes toward Br⁻

Figure 3.10 Cyclic voltammograms of **L1**/MWNTs modified glassy carbon electrode in pH 7 buffer solution (HEPES + NaClO$_4$) in the absence (solid line) and presence (dash line) of Br⁻ 1.0 mM, scan rate 100 mVs⁻¹.

After adding an excess Br⁻, the cyclic voltammogram showed insignificant changes of both anodic and cathodic waves suggesting that there was no interaction between Br⁻ and ligand **L1** modified MWNTs.

3.4.2.4 Cyclic Voltammetric Response of L1/MWNTs Modified GC Electrodes toward I⁻
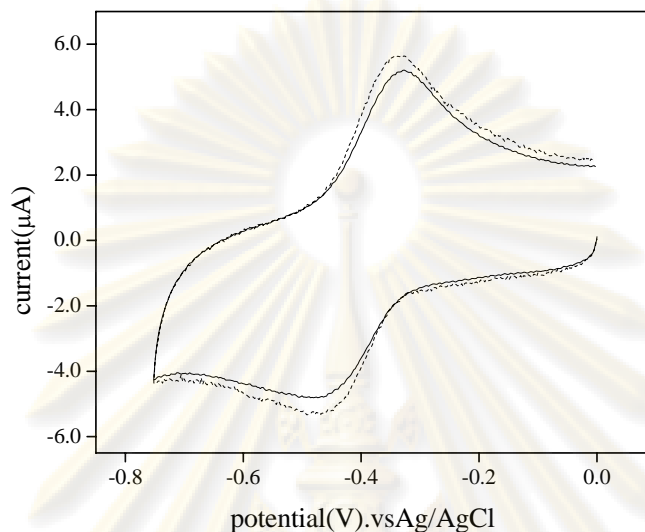

Figure 3.11 Cyclic voltammograms of **L1**/MWNTs modified glassy carbon electrode in pH 7 buffer solution (HEPES + NaClO₄) in the absence (solid line) and presence (dash line) of I⁻ 1.0 mM, scan rate 100 mVs⁻¹.

After adding an excess I⁻, the cyclic voltammogram showed insignificant changes of both anodic and cathodic waves suggesting that there was no interaction between I⁻ and ligand **L1** modified MWNTs.

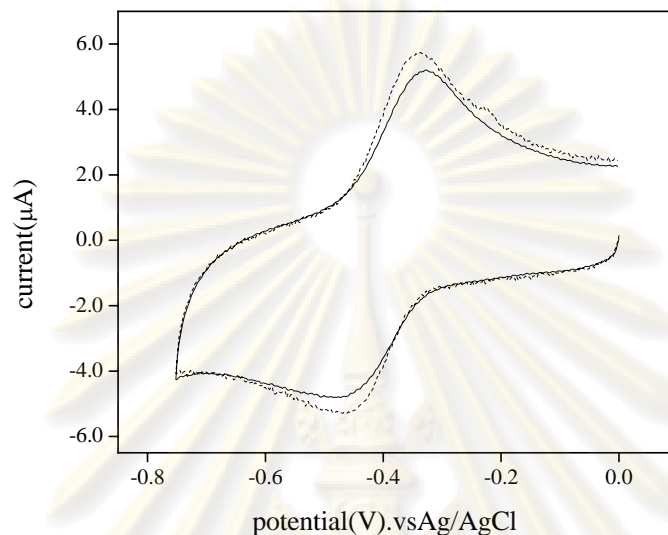### 3.4.2.5 Cyclic Voltammetric Response of L1/MWNTs Modified GC Electrodes toward $H_2PO_4^-$

Figure 3.12 Cyclic voltammograms of **L1**/MWNTs modified glassy carbon electrode in pH 7 buffer solution (HEPES + $NaClO_4$) in the absence (solid line) and presence (dash line) of $H_2PO_4^-$ 1.0 mM, scan rate 100 mVs^{-1}.

After adding an excess $H_2PO_4^-$, the cyclic voltammogram showed insignificant changes of both anodic and cathodic waves suggesting that there was no interaction between $H_2PO_4^-$ and ligand **L1** modified MWNTs.

3.4.3 Cyclic Voltammetric Response of L1/MWNTs Modified GC Electrodes toward Amino Acids

Considering the structure of **L1**, it comprised of anthraquinone dianion and imidazolium moieties, in which may appropriate for an amino acid containing both active groups of amine and carboxylic acid. Then, we studied on amino acids, such as glycine, D-alanine, D-leucine, D-phenylalanine and D-tryptophan. Unfortunately, the results presented the insignificant changes of anodic and cathodic currents indicating that no interactions occurred. This could be accounted for the reason previously mentioned in the anionic section.

3.4.3.1 Cyclic Voltammetric Response of L1/MWNTs Modified GC Electrodes toward Glycine
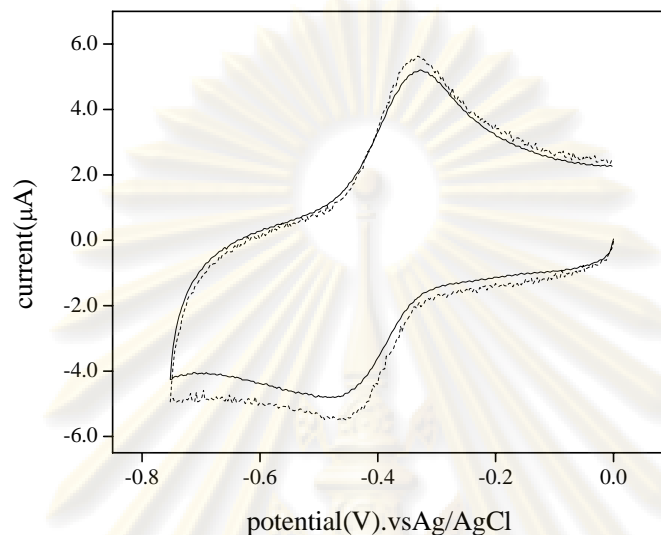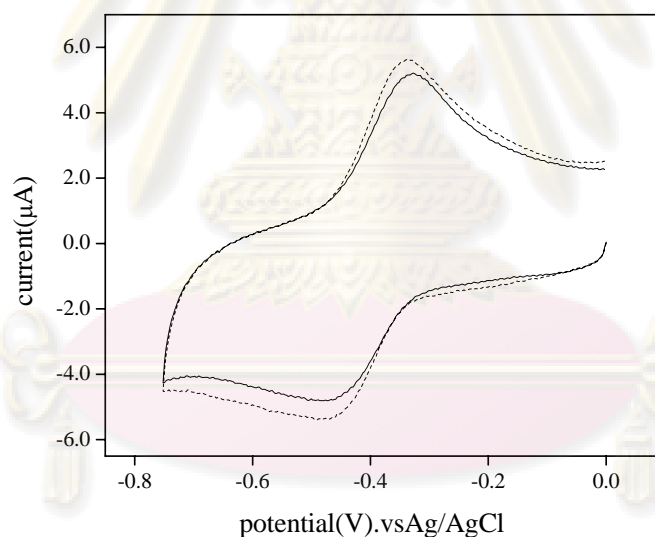

Figure 3.13 Cyclic voltammograms of **L1**/MWNTs modified glassy carbon electrode in pH 7 buffer solution (HEPES + NaClO$_4$) in the absence (solid line) and presence (dash line) of glycine 1.0 mM, scan rate 100 mVs^{-1}.

After adding an excess glycine, the cyclic voltammogram showed insignificant changes of both anodic and cathodic waves suggesting that there was no interaction between glycine and ligand **L1** modified MWNTs.

3.4.3.2 Cyclic Voltammetric Response of L1/MWNTs Modified GC Electrodes toward D-Alanine

Figure 3.14 Cyclic voltammograms of **L1**/MWNTs modified glassy carbon electrode in pH 7 buffer solution (HEPES + NaClO$_4$) in the absence (solid line) and presence (dash line) of D-alanine 1.0 mM, scan rate 100 mVs^{-1}.

After adding an excess D-alanine, the cyclic voltammogram showed insignificant changes of both anodic and cathodic waves suggesting that there was no interaction between D-alanine and ligand **L1** modified MWNTs.
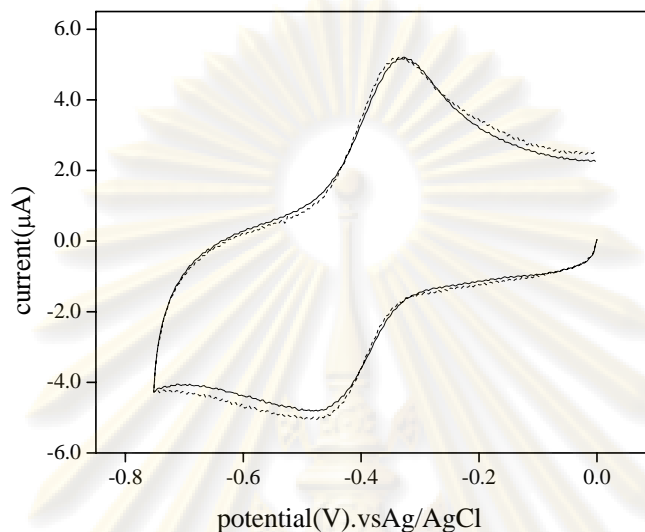
3.4.3.3 Cyclic Voltammetric Response of L1/MWNTs Modified GC Electrodes toward D-Leucine

Figure 3.15 Cyclic voltammograms of **L1**/MWNTs modified glassy carbon electrode in pH 7 buffer solution (HEPES + NaClO$_4$) in the absence (solid line) and presence (dash line) of D-leucine 1.0 mM, scan rate 100 mVs^{-1}.

After adding an excess D-leucine, the cyclic voltammogram showed insignificant changes of both anodic and cathodic waves suggesting that there was no interaction between D-leucine and ligand **L1** modified MWNTs.

3.4.3.4 Cyclic Voltammetric Response of L1/MWNTs Modified GC Electrodes toward D-Phenylalanine
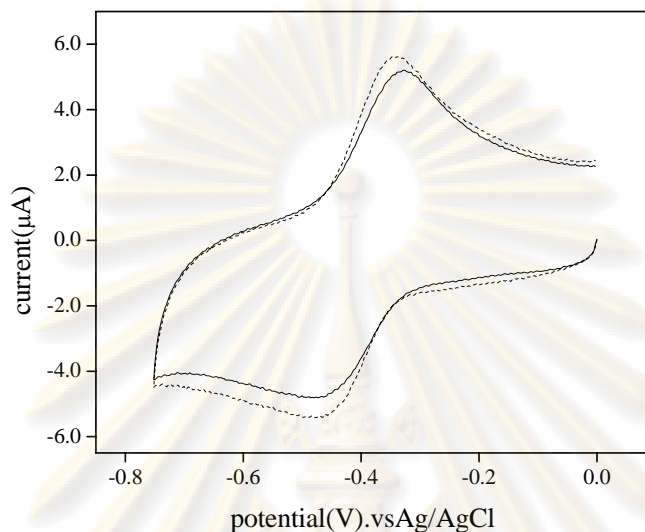

Figure 3.16 Cyclic voltammograms of **L1**/MWNTs modified glassy carbon electrode in pH 7 buffer solution (HEPES + NaClO$_4$) in the absence (solid line) and presence (dash line) of D-phenylalanine 1.0 mM, scan rate 100 mVs^{-1}.

After adding an excess D-phenylalanine, the cyclic voltammogram showed insignificant changes of both anodic and cathodic waves suggesting that there was no interaction between D-phenylalanine and ligand **L1** modified MWNTs.

3.4.3.5 Cyclic Voltammetric Response of L1/MWNTs Modified GC Electrodes toward D-Tryptophan
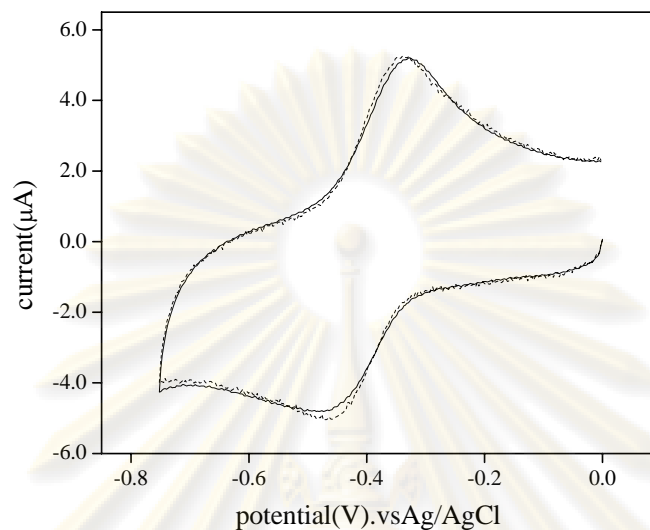

Figure 3.17 Cyclic voltammograms of **L1**/MWNTs modified glassy carbon electrode in pH 7 buffer solution (HEPES + NaClO$_4$) in the absence (solid line) and presence (dash line) of D-tryptophan 1.0 mM, scan rate 100 mVs^{-1}.

After adding an excess D-tryptophan, the cyclic voltammogram showed insignificant changes of both anodic and cathodic waves suggesting that there was no interaction between D-tryptophan and ligand **L1** modified MWNTs.

3.4.4 Cyclic Voltammetric Response of L1/MWNTs Modified GC Electrodes toward L-Cysteine

As a result of unsuccessful attempts, therefore, we intended to study on the electrocatalytic oxidation of L-cysteine (CySH). Typically, the direct oxidation of L-cysteine at conventional electrodes requires a large overpotential to be effective. According to the literature, we found glassy carbon electrode modified with multi-walled carbon nanotubes and poly(aminoquinone) could catalyze CySH oxidation with decrease in overpotential (0.26 V compared with bare GC). Cyclic voltammogram was observed in a range of -0.1 to 0.5 V. It appeared the oxidation peak at 0.28 V due to a couple of quinone/hydroquinone [56].

Since ligand **L1** contained anthraquinone derivative, it was expected to promote the electron-transfer reactions. Thus, we studied the electrocatalytic properties of **L1**/MWNTs modified glassy carbon electrodes toward L-cysteine by cyclic voltammetry in the potential range of 0.0 to 0.5 V. In the absence of cysteine, the experimental result exhibited a small bump at 0.14 V possibly caused by the oxidation of sodium perchlorate. To avoid the interference of sodium perchlorate, the buffer solution was changed to HEPES and sodium chloride (pH 7). In the absence of CySH, the bump at 0.14 V disappeared. Therefore, the electrocatalytic behavior of **L1** toward L-cysteine was carried out in HEPES and NaCl. Nevertheless, the cyclic voltammogram changed slightly in the addition of an excess CySH, shown in Figure 3.18.
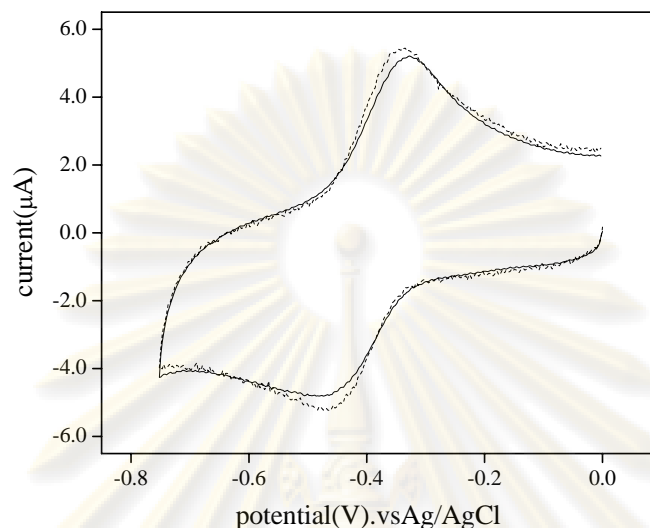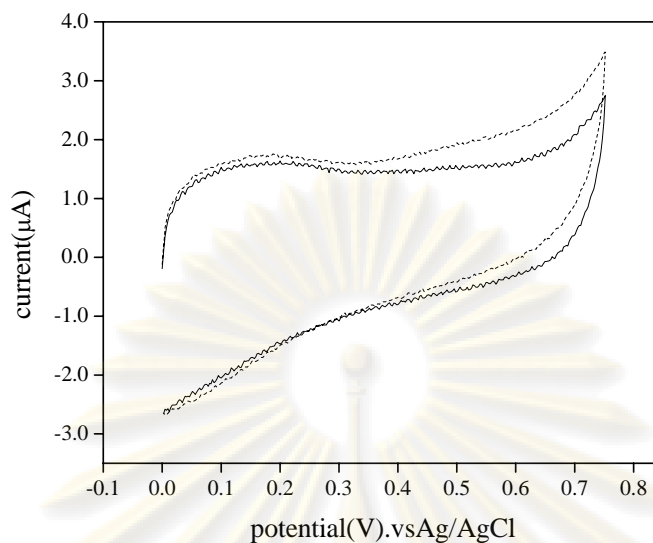
Figure 3.18 Cyclic voltammograms of **L1**/MWNTs modified glassy carbon electrode in pH 7 buffer solution (HEPES + NaCl) in the absence (solid line) and presence (dash line) of L-cysteine 0.5 mM, scan rate 100 mVs^{-1}.

3.4.5 Cyclic Voltammetric Response of L1/MWNTs Modified GC Electrodes toward Hydrazine

Hydrazine is one of reagents that have been attractive to many scientists due to its toxicities to human being. Since the oxidation of hydrazine also requires relative high overpotential at carbon electrodes, large numbers of approaches have been investigated to minimize this overpotential problem. It was suggested that the functionalization of glassy carbon electrodes with MWNTs and catechol derivatives could be used for the amperometric detection of hydrazine at reduced overpotential [57]. Thus, the electrochemical properties of **L1**/MWNTs modified GC electrodes over hydrazine was proceeded in the same condition, pH 7 buffer solution and the potential range 0.0 to 0.5 V. Obviously, the remarkable change of the anodic current was observed (Figure 3.19). To verify further the catalytic responses of **L1**/MWNTs modified GC toward hydrazine, cyclic voltammetric titrations were undertaken. Figure 3.20 represented the cyclic voltammograms of hydrazine titration over GC electrode modified with **L1**/MWNTs, in a range of hydrazine concentration 0.0 to 10.0 µM.
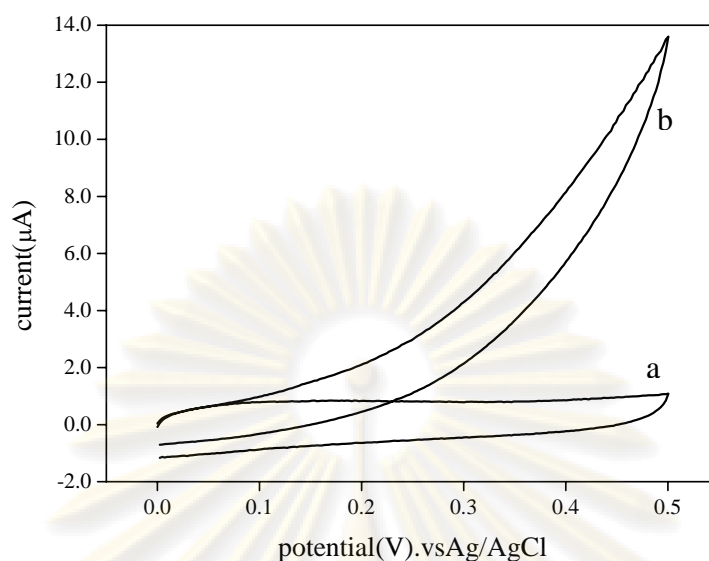
Figure 3.19 Cyclic voltammograms of **L1**/MWNTs modified GC electrode in pH 7 buffer solution (HEPES + NaCl) in (a) the absence and (b) presence of hydrazine 10.0 μM, scan rate 100 mVs^{-1}.
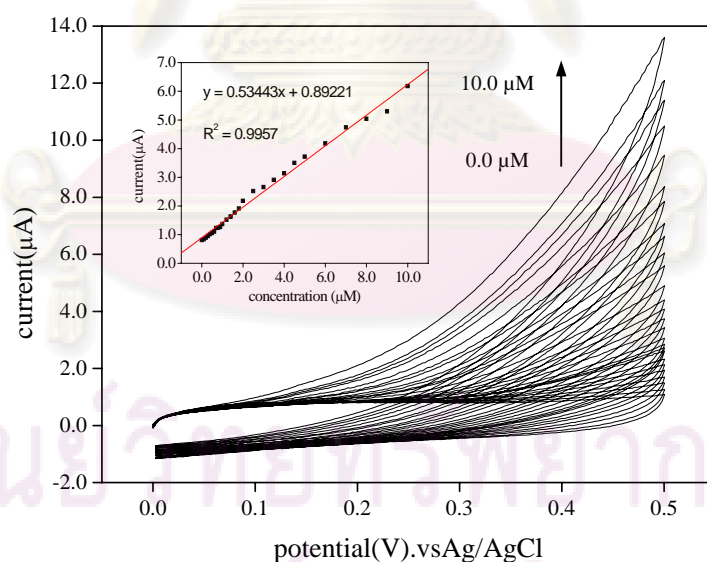
Figure 3.20 Cyclic voltammograms of **L1**/MWNTs modified GC electrode in pH 7 buffer solution (HEPES + NaCl) at different concentration of hydrazine (0.0-10.0 μM), scan rate 100 mVs^{-1}. Inset shows the variation of the electrocatalytic current vs. the concentration of hydrazine.
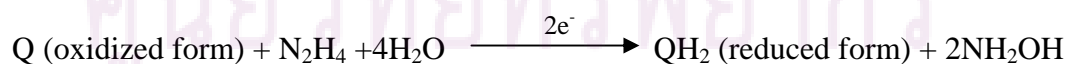
From Figure 3.20, the experimental result showed a linear correlation between catalytic currents and the concentration of hydrazine in the range of 0.0-10.0 μM, giving rise to a calibration plot for determining a detection limit (inset Figure 3.20). According to the method mentioned in the introduction [51], the detection limit of hydrazine of 1.01 μM was obtained. The values calculated from two experiments were slightly different, possibly caused by the uncertain fabrication resulting in unequal distribution of attached anthraquinone.

According to the literature, two assumptions corresponding to hydrazine oxidation have been proposed. The researchers suggest that a number of electrons involving in the oxidation of hydrazine are two and four [35, 58], represented in the following equations.

$$N_2H_4 + 4H_2O \rightleftharpoons 2NH_2OH + 2H_3O^+ + 2e^- \tag{1}$$

$$N_2H_4 + 4H_2O \rightleftharpoons N_2 + 4H_3O^+ + 4e^- \tag{2}$$
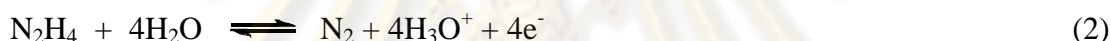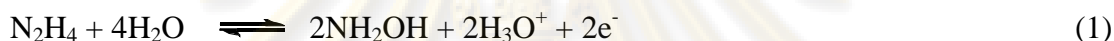
As shown in Eq. (1), hydrazine is transferred to hydroxylamine, and two electrons are generated. Conversely, hydrazine produces nitrogen gas and four electrons in Eq. (2)

Based on the results of cyclic voltammetric titration in the present research, it could not precisely conclude the number of electrons occurring from the oxidation process. The further investigations are required. Although the catalytic mechanism was not clearly defined, herein we proposed the following catalytic schemes to describe the electrocatalytic mechanism of hydrazine oxidation at **L1**/MWNTs modified GC electrodes.

$$Q \text{ (oxidized form)} + N_2H_4 + 4H_2O \xrightarrow{2e^-} QH_2 \text{ (reduced form)} + 2NH_2OH$$

$$QH_2 \text{ (reduced form)} \longrightarrow Q \text{ (oxidized form)} + 2e^- + 2H_3O^+$$

or

$$2Q \text{ (oxidized form)} + N_2H_4 + 4H_2O \xrightarrow{4e^-} 2QH_2 \text{ (reduced form)} + N_2$$

$$QH_2 \text{ (reduced form)} \longrightarrow Q \text{ (oxidized form)} + 2e^- + 4H_3O^+$$
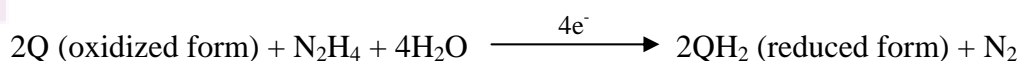
The preceding catalytic schemes imply that quinone attached to the electrode surface chemically reacts with hydrazine and the subsequent oxidation of hydroquinone regenerates anthraquinone, illustrated by Scheme 3.3. The large anodic current without the cathodic counterpart shown in the results is associated with hydrazine oxidation not hydroquinone, because the oxidation peak of hydroquinone was not observed.
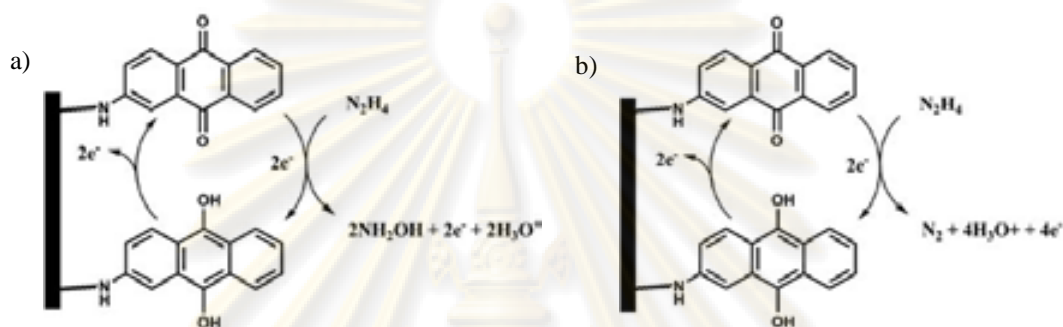
Scheme 3.3 Schematic diagrams of **L1**/MWNTs modified GC electrodes for the electrocatalytic oxidation of hydrazine. A number of electrons involving in hydrazine oxidation are two and four (a, b).

Additionally, the proposed catalytic mechanisms were analyzed by performing cyclic voltammetry with the used electrode. After finished hydrazine titration, the same electrode was rinsed with distilled water and then immersed in buffer solution. The potential was firstly cycled between 0.0-0.5 V, and the voltammogram showed no significant response (Figure 3.21). This result was a good agreement with the electrocatalytic schemes suggesting that the reaction between hydrazine and anthraquinone regenerated quinone compound. After that, we tried to prove the existence of anthraquinone, the potential range of -0.75 to 0.0 V was then applied. We observed the characteristic redox waves of Q/QH_2 system, as expected for the reduction of anthraquinone (Figure 3.22).
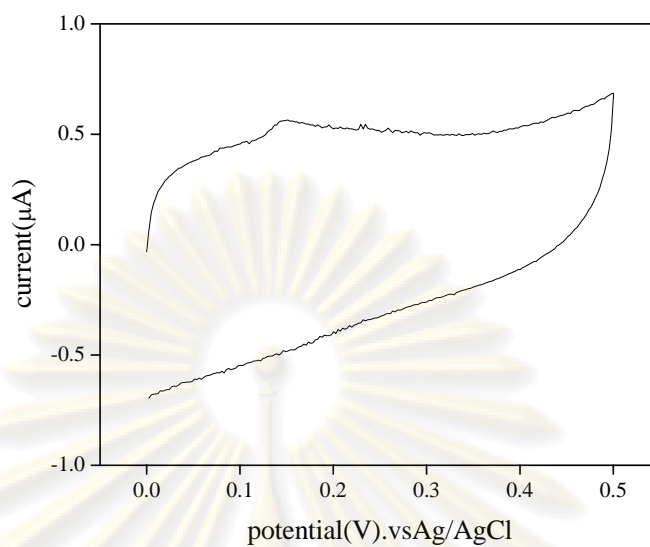
Figure 3.21 Cyclic voltammogram of used **L1**/MWNTs modified GC electrode in pH 7 buffer solution (HEPES + NaCl), scan rate 100 mVs^{-1}.
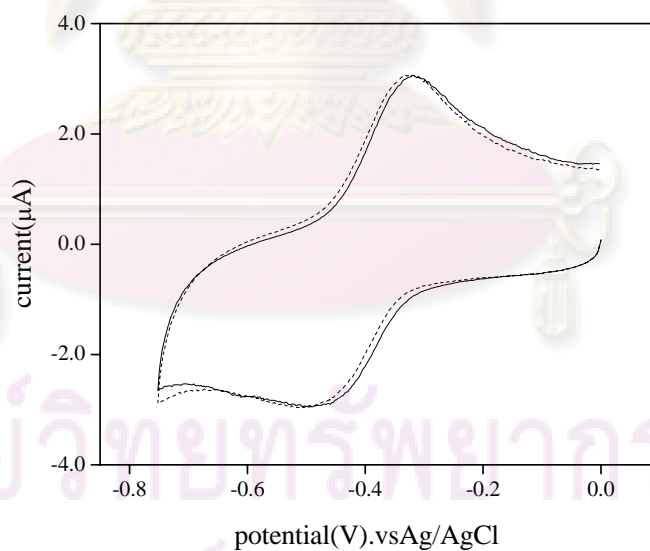
Figure 3.22 Cyclic voltammograms of **L1**/MWNTs modified GC electrode in pH 7 buffer solution (HEPES + NaCl). Freshly prepared electrode (solid line) and used electrode (dash line), scan rate 100 mVs^{-1}.

3.4.6 Cyclic Voltammetric Response of Bare GC Electrodes toward Hydrazine
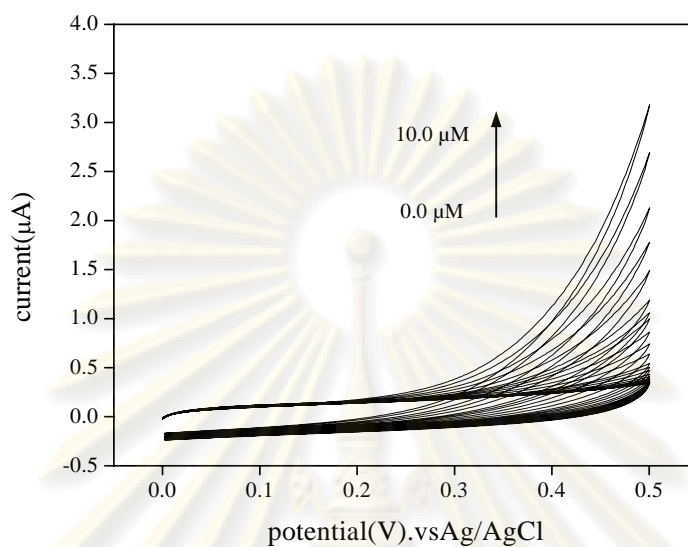
Figure 3.23 Cyclic voltammograms of GC electrode in pH 7 buffer solution (HEPES + NaCl) at different concentration of hydrazine (0.0-10.0 μM), scan rate 100 mVs^{-1}.
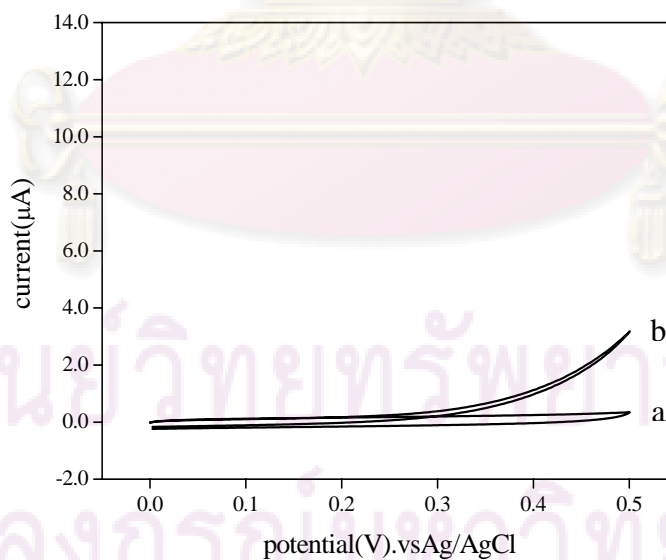
Figure 3.24 Cyclic voltammograms of GC electrode in pH 7 buffer solution (HEPES + NaCl) in (a) the absence, and (b) presence of hydrazine 10.0 μM.

To compare the great electrocatalytic properties of **L1**/MWNTs modified electrodes and bare GC electrodes for hydrazine detection, the studies on the detection of hydrazine by GC electrodes were then performed. The cyclic voltammetric titrations of hydrazine at GC electrodes (shown in Figure 3.23) were carried out in the same condition. Figure 3.24 showed the cyclic voltammograms of bare GC electrode in the presence and the absence of hydrazine.

Compared to **L1**/MWNTs modified electrodes, the lower oxidative current (*ca.* four times lower than modified electrode) was obtained in the case of bare GC electrodes. Possibly, it was not reactive for hydrazine oxidation. In the previous works, research groups reported that modified electrodes could be used to promote electron transfer in the electrocatalytic oxidation of hydrazine [35-39, 59]. High sensitivity of modified electrodes was the extraordinary features of multi-walled carbon nanotubes due to the porous interfacial layer and the unique electrical property. Both internal and external surfaces of the nanotubes were the excellent surfaces for immobilizing synthesized compound, which led to more reactive than the bare electrodes.

3.4.7 Cyclic Voltammetric Response of MWNTs-COOH Modified GC Electrodes toward Hydrazine

Moreover, we analyzed the catalytic behavior of glassy carbon electrodes modified with carboxylated carbon nanotubes (MWNTs-COOH) toward hydrazine. It was found that MWNTs-COOH modified electrodes also acted as a mediator for hydrazine oxidation, but extremely large background current was observed (Figure 3.25). This suggested that **L1**/MWNTs modified electrodes were effective for the electrocatalytic oxidation of hydrazine with high sensitivity. The voltammograms obtained from hydrazine titration were presented in Figure 3.26.
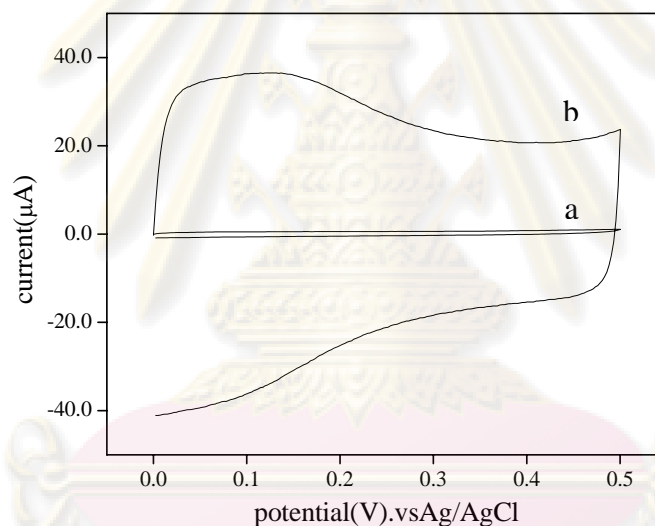
Figure 3.25 Cyclic voltammograms of (a) **L1**/MWNTs and (b) MWNTs-COOH modified GC electrodes in pH 7 buffer solution (HEPES + NaCl) in the absence of hydrazine.
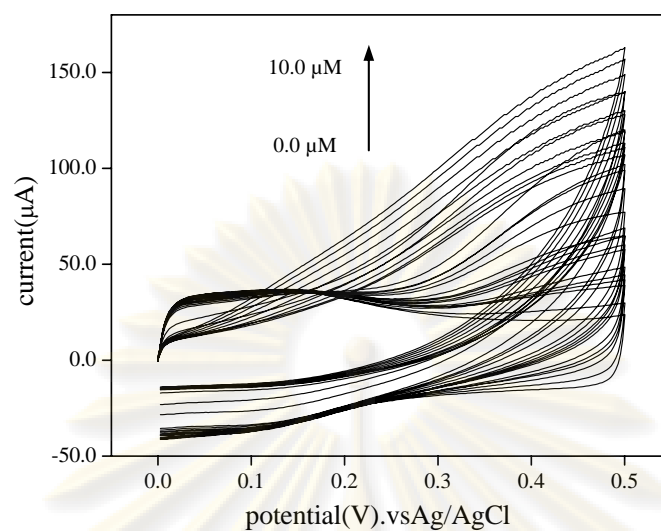
Figure 3.26 Cyclic voltammograms of MWNTs-COOH modified GC electrode in pH 7 buffer solution (HEPES + NaCl) at different concentration of hydrazine (0.0-10.0 μM), scan rate 100 mVs^{-1}.

3.4.8 Cyclic Voltammetric Response of L1/MWNTs Modified GC Electrodes toward Sodium Thiosulfate
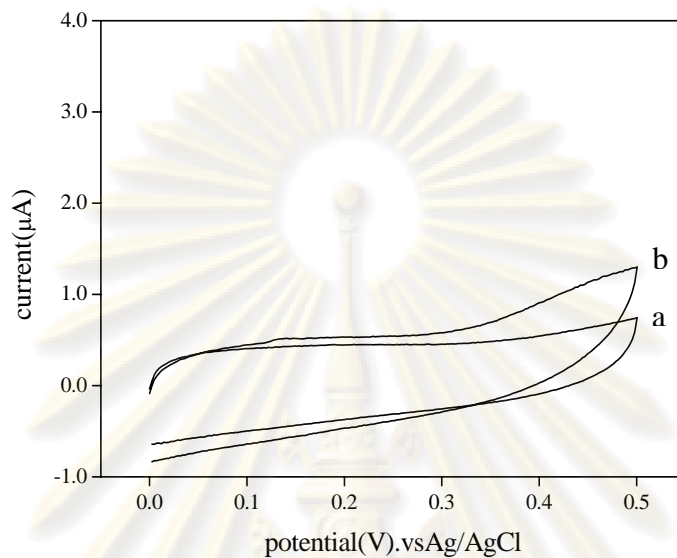

Figure 3.27 Cyclic voltammograms of **L1**/MWNTs modified GC electrode in pH 7 buffer solution (HEPES + NaCl) in (a) the absence and (b) presence of sodium thiosulfate 10.0 μM.
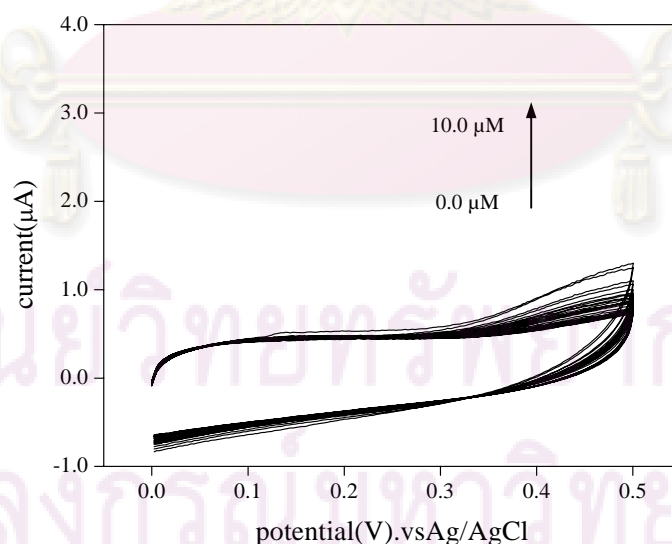

Figure 3.28 Cyclic voltammograms of **L1**/MWNTs modified GC electrode in pH 7 buffer solution (HEPES + NaCl) at different concentration of sodium thiosulfate (0.0-10.0 μM), scan rate 100 mVs^{-1}.

To ascertain that the obtained electrode has a selectivity to detect hydrazine, one more reducing agent was analyzed. The experiments conducted on sodium thiosulfate were presented in Figure 3.27 and Figure 3.28. The anodic current barely changed while adding the solution of sodium thiosulfate. Based on these results, it was implied that **L1**/MWNTs modified electrodes were unreactive in this condition.

3.4.9 Cyclic Voltammetric Response of Bare GC Electrodes toward Sodium Thiosulfate

Cyclic voltammetric titrations of sodium thiosulfate at bare GC electrodes were also investigated, shown in Figure 3.29. However, the change of catalytic current was not observed as well.
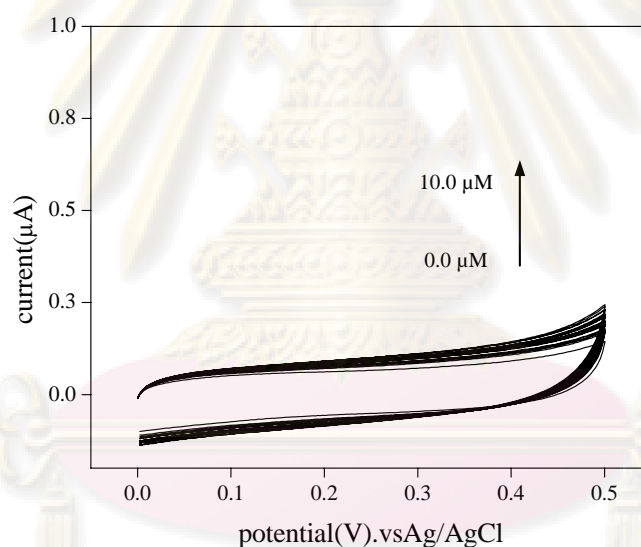

Figure 3.29 Cyclic voltammograms of GC electrode in pH 7 buffer solution (HEPES + NaCl) at different concentration of sodium thiosulfate (0.0-10.0 μM), scan rate 100 mVs^{-1}.

Eventually, Figure 3.30 verified that GC electrodes modified with **L1**/MWNTs exhibited promising behavior toward the electrocatalytic oxidation of hydrazine. A comparison between the bare electrodes and the modified electrodes, the latter showed many advantages for hydrazine detection, including low detection limit and high sensitivity.
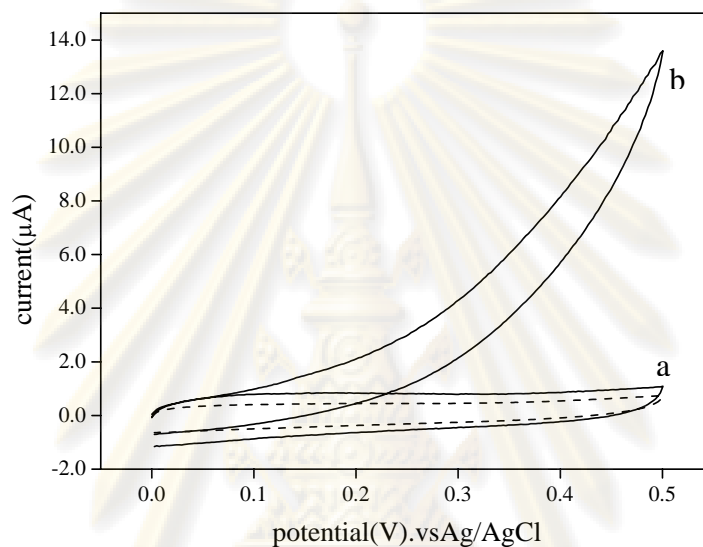
Figure 3.30 Cyclic voltammograms of **L1**/MWNTs modified GC electrode in pH 7 buffer solution (HEPES + NaCl) in (a) the absence and (b) presence of hydrazine 10.0 μM, compared with bare GC electrode in 10.0 μM hydrazine solution (dash line).

CHAPTER IV

CONCLUSION

The synthetic pathway of anthraquinone derivative containing imidazolium salt **L1** has been illustrated herein. This synthesized ligand was immobilized onto multi-walled carbon nanotube surface via covalent modification, and the modified nanotubes were further fabricated to glassy carbon electrodes. Complexation studies toward various anions and amino acids were analyzed by cyclic voltammetry in pH 7 buffer solution (HEPES + NaCl). There were no changes of both cathodic and anodic currents indicating that **L1** modified nanotubes were non-selective to anions and amino acids. However, **L1**/MWNTs modified electrodes exhibited the exceptional characteristic as a hydrazine sensor at low concentration. It was apparent that **L1**/MWNTs modified electrodes showed higher sensitivity and lower background current for hydrazine detection compared with MWNTs-COOH GC electrodes. Moreover, electrodes attached with **L1**/MWNTs intensified the catalytic current about four times higher than bare GC electrodes. A detection limit of 1.01 µM was obtained from the linear range over hydrazine concentration 0.0-10.0 µM. According to the literature, we also proposed the catalytic schemes for the oxidation of hydrazine. At the electrode surface, hydrazine electrochemically reduced anthraquinone to hydroquinone and anthraquinone was regenerated by the subsequent oxidation of hydroquinone.

Suggestions for future work:

1. The further investigations including cyclic voltammetry at different scan rates and chronoamperometry are required to afford the rate-determining step and the number of electrons involved in hydrazine oxidation.
2. The catalytic response of modified electrodes toward hydrazine in a variety of pH values should be analyzed.

REFERENCES

[1]   Garrod, S.; Bollard, M. E.; Nicholls, A. W.; Connor, S. C.; Connelly, J.;
        Nicholson, J. K.; Holmes, E. Integrated Metabonomic Analysis of the
        Multiorgan Effects of Hydrazine Toxicity in the Rat. *Chem. Res.
        Toxicol*. 18 (2005) : 115-122.

[2]   Morris, J.; Densem, J. W.; Waid, N. J.; Doll, R. Occupational exposure to
        hydrazine and subsequent risk of cancer. *Occup. Environ. Med*. 52
        (1995) : 43-45.

[3]   Meyyappan, M. *Carbon Nanotubes: Science and Applications*. Florida: CRC
        Press, **2005**.

[4]   Rao, C. N. R.; Satishkumar, B. C.; Govindaraj, A.; Natch, M. Nanotubes.
        ChemPhysChem. 2 (2001) : 78-105.

[5]   Ajayan, P. M. Nanotubes from Carbon. *Chem. Rev*. 99 (1999) : 1787-1799.

[6]   Iijima, S. Helical microtubules of graphitic carbon. *Nature*. 354 (1991) : 56-58.

[7]   Dresselhaus, M. S.; Dresselhaus, G.; Eklund, P. C. *Science of Fullerene and
        Carbon Nanotubes*. New York: Academic Press, **1996**.

[8]   Ebbesen, T. W. Carbon Nanotubes. *Physics Today*. 49 (1996) : 26-32.

[9]   Hu, H.; Zhao, B.; Itkis, M. E.; Haddon, R. C. Nitric Acid Purification of Single
        Single-Walled Carbon Nanotubes. J. *Phys. Chem. B*. 107 (2003) :
        13838-13842.

[10]   Lin, Y.; Rao, A. M.; Sadanadan, B.; Kenik, E. A.; Sun, Y. Functionalizing
        Multiple-Walled Carbon Nanotubes with Aminopolymers. *J. Phys.
        Chem. B*. 106 (2002) : 1294-1298.

[11]   Alvaro M.; Arile, C.; Ferrer, B.; Garcia, H. Functional Molecules from Single
        Wall Carbon Nanotubes. Photoinduced Solubility of Short Single
        Wall Carbon Nanotubes Residues by Covalent Anchoring of 2,4,6-
        Triarylpyrylium Units. *J. Am. Chem. Soc*. 129 (2007) : 5647-5655.

[12]   Aitchison, T. J.; Ginic-Markovic, M.; Matisons, J. G.; Simon, G. P.; Fredericks,
        P. M. Purification, Cutting, and Sidewall Functionalization of
        Multiwalled Carbon Nanotubes Using Potassium Permanganate
        Solutions. *J. Phys. Chem. C*. 111 (2007) : 2440-2446.

[13] Ziegler, K. J.; Gu, Z.; Peng, H.; Flor, E. L.; Hauge, R. H.; Smalley, R. E. Controlled Oxidative Cutting of Single-Walled Carbon Nanotubes. *J. Am. Chem. Soc*. 127 (2005) : 1541-1547.

[14] Banerjee, S.; Wong, S. S. Rational Sidewall Functionalization and Purification of Single-Walled Carbon Nanotubes by Solution-Phase Ozonolysis. *J. Phys. Chem. B*. 106 (2002) : 12144-12151.

[15] Park, M. J.; Lee, J. K.; Lee, B. S.; Lee, Y.; Choi, I. S.; Lee, S. Covalent Modi-fication of Multiwalled Carbon Nanotubes with Imidazolium-Based Ionic Liquids: Effect of Anions on Solubility. *Chem. Mater*. 18 (2006) : 1546-1551.

[16] Yu, B.; Zhou, F.; Liu, G.; Liang, Y.; Huck, W. T. S.; Liu, W. The electrolyte switchable solubility of multi-walled carbon nanotube/ionic liquid (MWCNT/IL) hybrids. *Chem. Commun*. (2006) : 2356-2358.

[17] D'Souza, F.; Chitta, R.; Sandanayaka, A. S. D.; Subbaiyan, N. K.; D'Souza, L.; Araki, Y.' Ito, O. Supramolecular Carbon Nanotube-Fullerene Donor-Acceptor Hybrids for Photoinduced Electron Transfer. *J. Am. Chem. Soc*. 129 (2007) : 15865-15871.

[18] Piao, L.; Liu, Q.; Li, Y.; Wang, C. Adsorption of L-Phenylalanine on Single-Walled Carbon Nanotubes. *J. Phys. Chem. C*. 112 (2008) : 2857-2863.

[19] Witus, L. S.; Rocha, J. R.; Yuwono, V. M.; Paramonov, S. E.; Weisman, R. B.; Hartgerink, J. D. Peptides that non-covalently functionalize single-walled carbon nanotubes to give controlled solubility characteristics. *J. Mater. Chem*. 17 (2007) : 1909-1915.

[20] Zhao, B.; Hu, H.; Haddon, R. C. Synthesis and Properties of a Water-Soluble Single-Walled Carbon Nanotube-Poly(*m*-aminobenzene sulfonic acid) Graft Copolymer. *Adv. Funct. Mater*. 14 (2004) : 71-76.

[21] Ke, G.; Guan, W. C.; Tang, C. Y.; Hu, Z.; Guan, W. J.; Zeng, D. L.; Deng, F. Covalent modification of multiwalled carbon nanotubes with a low molecular weight chitosan. *Chinese Chem. Lett*. 18 (2007) : 361-364.

[22] Wang, J.; Deo, R. P.; Musameh, M. Stable and Sensitive Electrochemical Detection of Phenolic Compounds at Carbon Nanotube Modified Glassy Carbon Electrodes. *Electroanalysis*. 15 (2003) : 1830-1834.

[23] Tsai, Y.; Chen, J.; Marken, F. Simple Cast-Deposited Multi-Walled Carbon
      Nanotube/Nafion^{TM} Thin Film Electrodes for Electrochemical
      Stripping Analysis. *Microchim. Acta*. 15 (2005) : 269-276.

[24] Wu, W.; Zhu, H.; Fan, L.; Liu, D.; Renneberg, R.; Yang, S. Sensitive dopamine
      recognition acid functionalized multi-walled carbon nanotubes. *Chem.
      Commun*. (2007) : 2345-2347.

[25] Yang, X.; Lu, Y.; Ma, Y.; Liu, Z.; Du, F. DNA electrochemical sensor based on
      an adduct of single-walled carbon nanotubes and ferrocene.
      Biotechnol. Lett. 29 (2007) : 1775-1779.

[26] Zhang, H. Fabrication of a single-walled carbon nanotube-modified glassy
      carbon electrode and its application in the electrochemical
      determination of epirubicin. *J. Nanopart. Res*. 6 (2004) : 665-669.

[27] Dai, Y.; Shiu, K. Glucose Biosensor Based on Multi-Walled Carbon Nanotube
      Modified Glassy Carbon Electrode. *Electroanalysis*. 16 (2004) :
      1697-1703.

[28] So, H.; Won, K.; Kim, Y. H.; Kim, B.; Ryu, B. H.; Na, P. S.; Kim, H.; Lee, J.
      Single-Walled Carbon Nanotube Biosensors Using Aptamers as
      Molecular Recognition Elements. *J. Am. Chem. Soc*. 127 (2005) :
      11906-11907.

[29] Besteman, K.; Lee, J.; Wiertz, F. G. M.; Heering, H. A.; Dekker, C. Enzyme-
      Coated Carbon Nanotubes as Single-Molecule Biosensors. *Nano.
      Lett*. 3 (2003) : 727-730.

[30] Liu, G.; Lin, Y. Biosensor Based on Self-Assembling Acetylcholinesterase on
      Carbon Nanotubes for Flow Injection/Amperometric Detection of
      Organophosphate Pesticides and Nerve Agents. *Anal. Chem*. 78
      (2006) : 835-843.

[31] Lee, K. Y.; Kim, M.; Hahn, J.; Suh, J. S.; Lee, I.; Kim, K.; Han, S. W.
      Assembly of Metal Nanoparticle-Carbon Nanotube Composite
      Materials at Liquid/Liquid Interface. *Langmuir*. 22 (2006) : 1817-
      1821.

[32] Liu, Z.; Sun, X.; Nakayama-Ratchford, N.; Dai, H. Supramolecular Chemistry
      on Water-Soluble Carbon Nanotubes for Drug Loading and Delivery.

ACS Nano. 1 (2007) : 1.

[33] Ozoemena, K. I.; Nyokong, T. Electrocatalytic oxidation and detection of hydrazine at gold electrode modified with iron phthalocyanine complex linked to mercaptopyridine self-assembled monolayer. *Talanta*. 67 (2005) : 162-168.

[34] Niu, L.; You, T.; Gui, J. Y.; Wang, E.; Dong, S. Electrocatalytic oxidation of hydrazine at a 4-pyridyl hydroquinone self-assembled platinum electrode and its application to amperometric detection in capillary electrophoresis. *J. Electroanal. Chem.* 448 (1998) : 79-86.

[35] Zare, H. R.; Nasirizadeh, N. Hematoxylin multi-wall carbon nanotubes modified glassy carbon electrode for electrocatalytic oxidation of hydrazine. *Electrochim. Acta*. 52 (2007) : 4153-4160.

[36] Ensafi, A. A.; Mirmomtaz, E. Electrocatalytic oxidation of hydrazine with pyrogallol red as a mediator on glassy carbon electrode. *J. Electroanal. Chem*. 583 (2005) : 176-183.

[37] Scharf, U.; Grabner, E. W. Electrocatalytic oxidation of hydrazine at a Prussian blue-modified glassy carbon electrode. *Electrochim. Acta*. 41 (1996) : 233-239.

[38] Majidi, M. R.; Jouyban, A. J.; Asadpour-Zeynali, K. Electrocatalytic oxidation of hydrazine at overoxidized polypyrrole film modified glassy carbon electrode. *Electrochim. Acta*. 52 (2007) : 6248-6253.

[39] Ardakani, M. M.; Karami, P. E.; Rahimi, P.; Zare, H. R.; Naeimi, H. Electrocatalytic hydrazine oxidation on quinizarine modified glassy carbon electrode. *Electrochim. Acta*. 52 (2007) : 6118-6124.

[40] Nassef, H. M.; Radi, A.; O'Sullivan, C. K. Electrocatalytic oxidation of hydrazine at *o*-aminophenol grafted modified glassy carbon electrode: Reusable hydrazine amperometric sensor. *J. Electroanal. Chem*. 592 (2006) : 139-146.

[41] Christie, R. M. *Colour chemistry*. Cambridge: Royal Society of Chemistry, **2001**.

[42] Wightman, R. M.; Cockrell, J. R.; Murray, R. W.; Burnett, J. N. Protonation Kinetics and Mechanism for 1,8-Dihydroxyanthraquinone and Anthraquinone Anion Radicals in Dimethylformamide Solvent. *J.*

Am. Chem. Soc. 98 (1976) : 2562-2570.

[43]   Steed, J. W.; Turner, D. R.; Wallace, K. J. *Core Concepts in Supramolecular Chemistry and Nanochemistry*. Chichester: John Wiley & Sons, **2007**.

[44]   Devaraj, S.; Saravanakumar, D.; Kandaswamy, M. Dual chemosensing properties of new anthraquinone-based receptors toward fluoride ions. *Tetrahedron Lett*. 48 (2007) : 3077-3081.

[45]   Banks, C. E.; Wildgoose, G. G.; Heald, C. G. R.; Compton, R. G. Oxygen Reduction Catalysis at Anthraquinone Centres Molecularly Wired *Via* Carbon Nanotubes. *J. Iranian Chem. Soc*. 2 (2005) : 60-64.

[46]   Gale, P. A. Anion and ion-pair receptor chemistry: highlights from 2000 and 2001. *Coord. Chem. Rev*. 240 (2003) : 191-221.

[47]   Yoon, J.; Kim, S. K.; Singh, N. J.; Lee, J. W. Yang, Y. J.; Chellappan, K.; Kim, K. S. Highly Effective Fluorescent Sensor for $H_2PO_4^-$. *J. Org. Chem*. 69 (2004) : 581-583.

[48]   Bargossi, C.; Fiorini, M. C.; Montalti, F. M.; Prodi, L.; Zaccheroni, N. Recent developments in transition metal ion detection by luminescent chemosensors. *Coord. Chem. Rev*. 208 (2000) : 17-32.

[49]   Wang, J. *Analytical Electrochemistry*. New Jersey: John Wiley & Sons, **2006**.

[50]   Sawyer, D. T.; Sobkowiak, A.; Roberts, Jr. J. L. *Electrochemistry for chemists*. New York: John Wiley & Sons, **1995**.

[51]   Miller, J. N.; Miller, J. C. *Statistics and chemometrics for analytical chemistry*. Harlow: Prentice Hall, **2000**.

[52]   Kim, S. K.; Seo, D.; Han, S. J.; Son, G.; Lee, I. Lee, C. Lee, K. D.; Yoon, J. A new imidazolium acridine derivative as fluorescent chemosensor for pyrophosphate and dihydrogen phosphate. *Tetrahedron*. 64 (2008) : 6402-6405.

[53]   Thomas, J. Howarth, J.; Hanlon, K.; McGuirk, D. Ferrocenyl imidazolium salts as a new class of anion receptors with C-H···X⁻ hydrogen bonding. *Tetrahedron Lett*. 41 (2000) : 413-416.

[54]   Ramanathan, T.; Fisher, F. T.; Ruoff, R. S.; Brinson, L. C. Amino-Functionalized Carbon Nanotubes for Binding to Polymers and Biological Systems. *Chem. Mater*. 17 (2005) : 1290-1295.

[55]   Zhu, Z.; Li, N. 9,10-Anthraquinone Modified Glassy Carbon Electrode and Its Application for Hemoglobin Determination. *Electroanalysis*. 10 (1998) : 643-646.

[56]   Tu, X.; Xie, Q.; Huang, Z.; Jia, X.; Ye, M. Electrocatalytic oxidation and sensitive determination of L-cysteine at a poly(aminoquinone)-carbon nanotubes hybrid film modified glassy carbon electrode. Microchim. Acta. 162 (2008) : 219-225.

[57]   Salimi, A.; Miranzadeh, L.; Hallaj, R. Amperometric and voltammetric detection of hydrazine using glassy carbon electrodes modified with carbon nanotubes and catechol derivatives. *Talanta*. 75 (2008) : 147-156.

[58]   Zare, H. R.; Habibirad, A. M. Electrochemistry and electrocatalytic activity of catechin film on a glassy carbon electrode toward the oxidation of hydrazine. J. *Solid. State Electrochem*. 10 (2006) : 348-359.

[59]   Ozoemena, K. I. Anodic Oxidation and Amperometric Sensing of Hydrazine at a Glassy Carbon Electrode Modified with Cobalt (II) Phthalocyanine-cobalt (II) Tetraphenylporphyrin (CoPc-(CoTPP)$_4$). *Sensors*. 6 (2006) : 874-891.
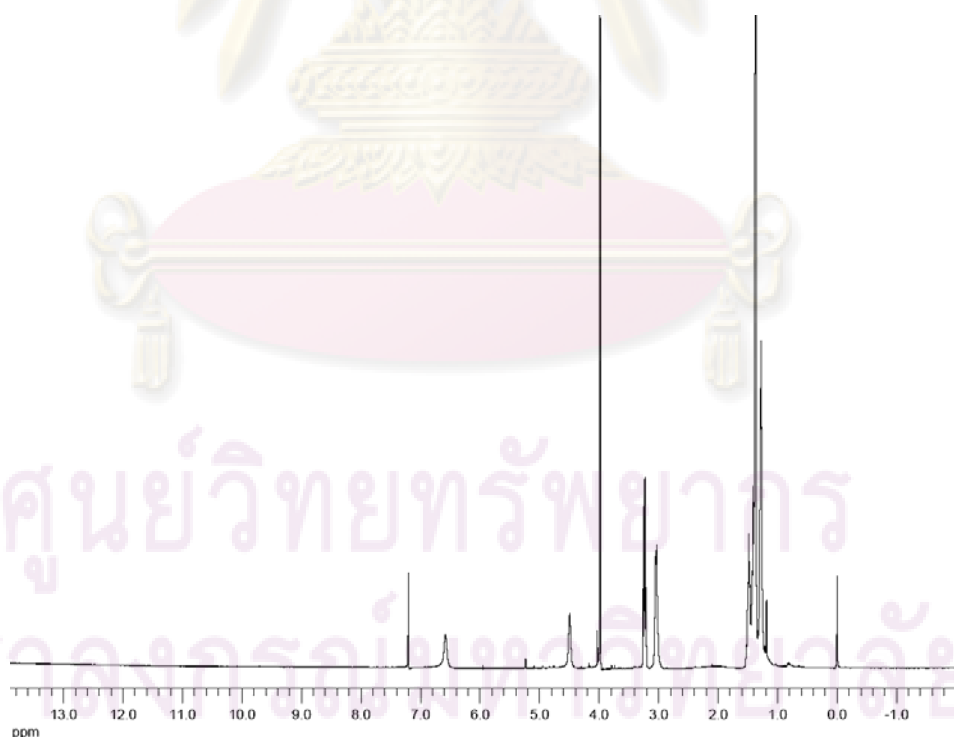
APPENDICES
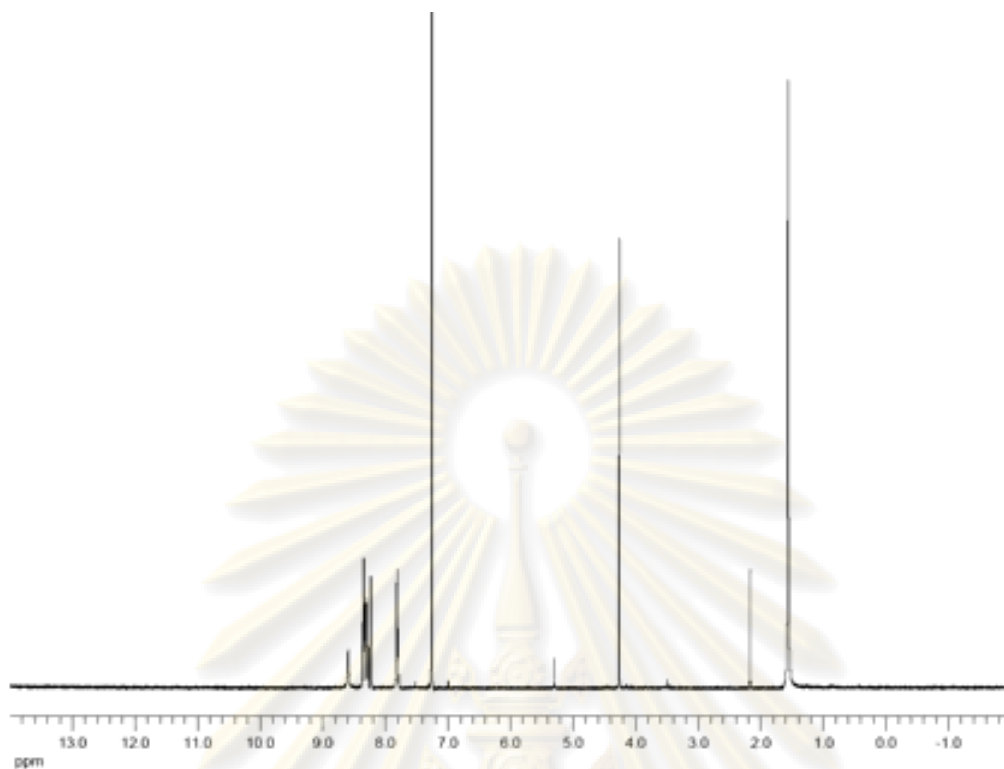
Figure A.1 The ^{1}H-NMR spectrum of 2-(2-chloroacetamido)anthracene-9,10-dione **(1)** in CDCl$_3$ with 400 MHz.
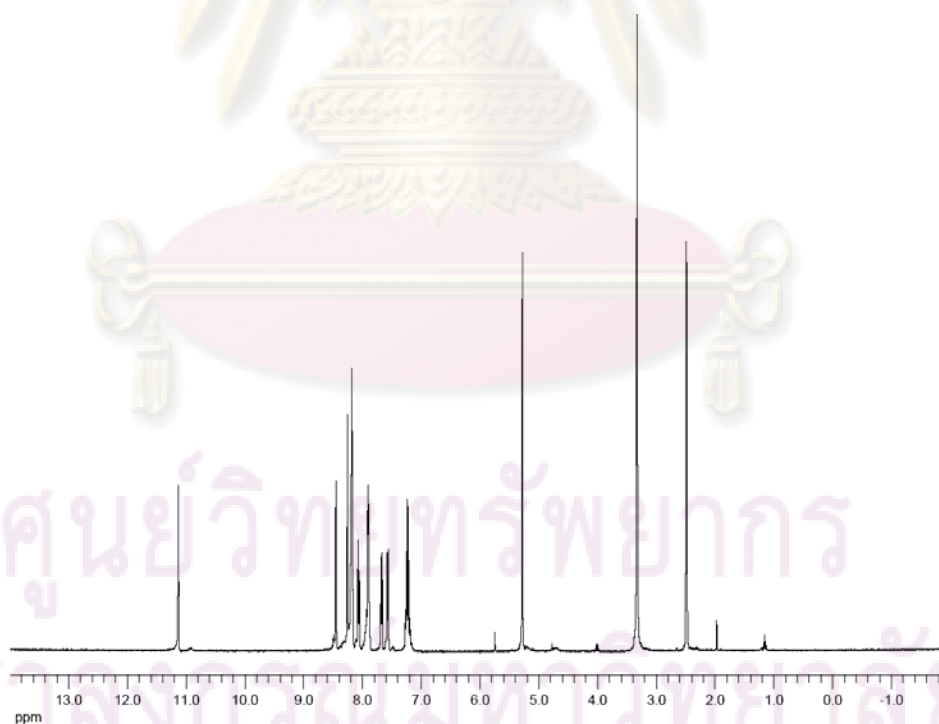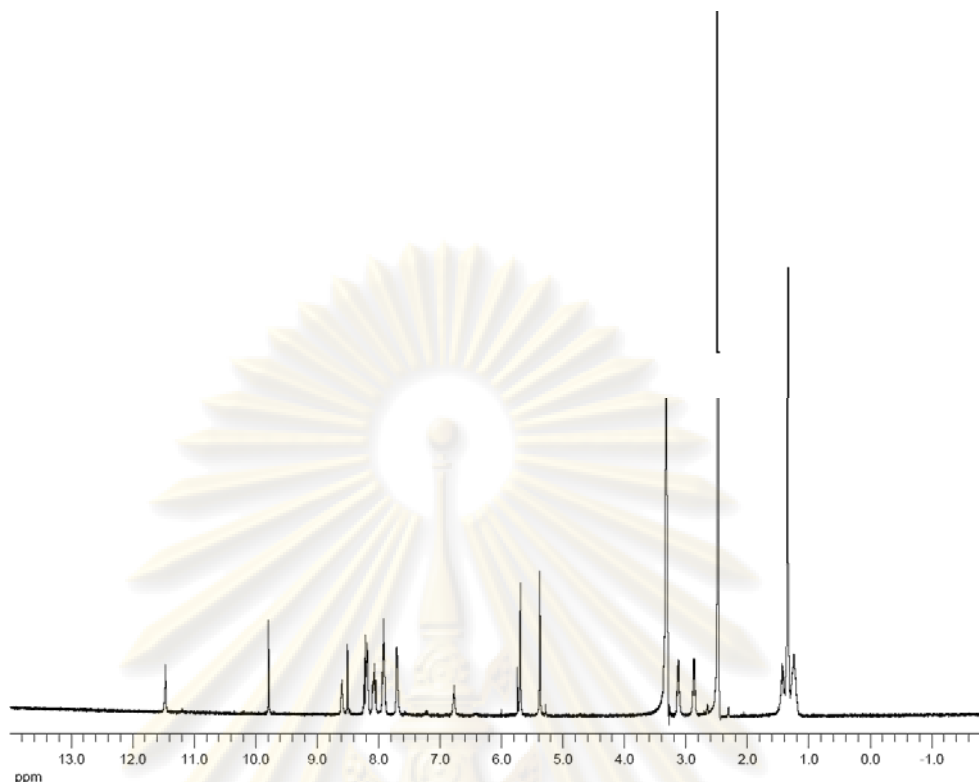

Figure A.2 The ^{1}H-NMR spectrum of 2-(benzimidazole-1-acetamido)anthracene-9,10-dione **(2)** in DMSO-d6 with 400 MHz.
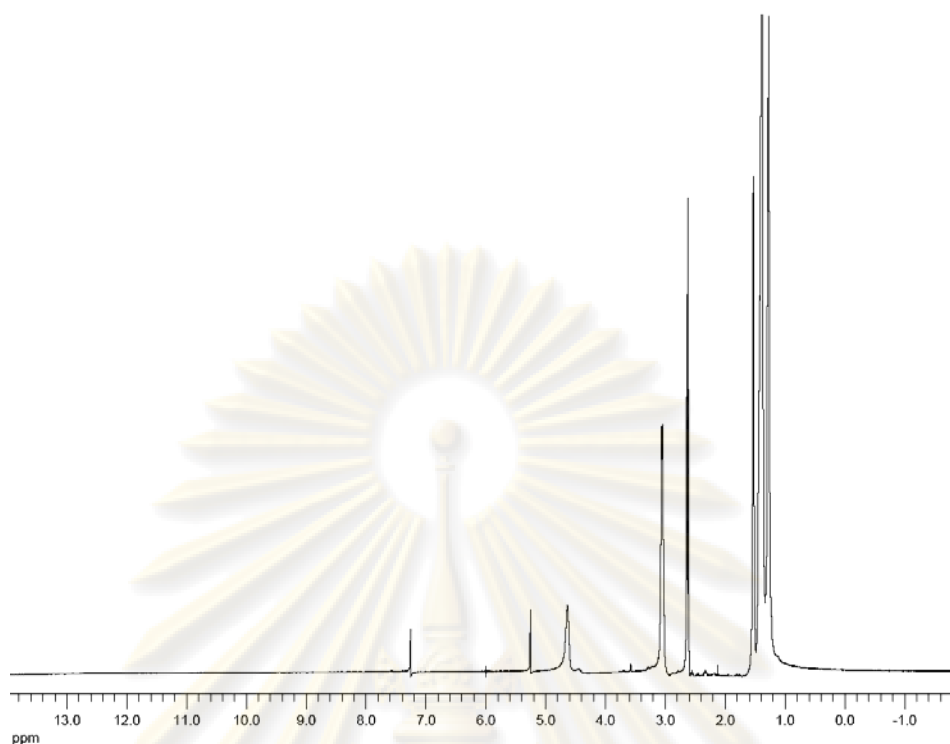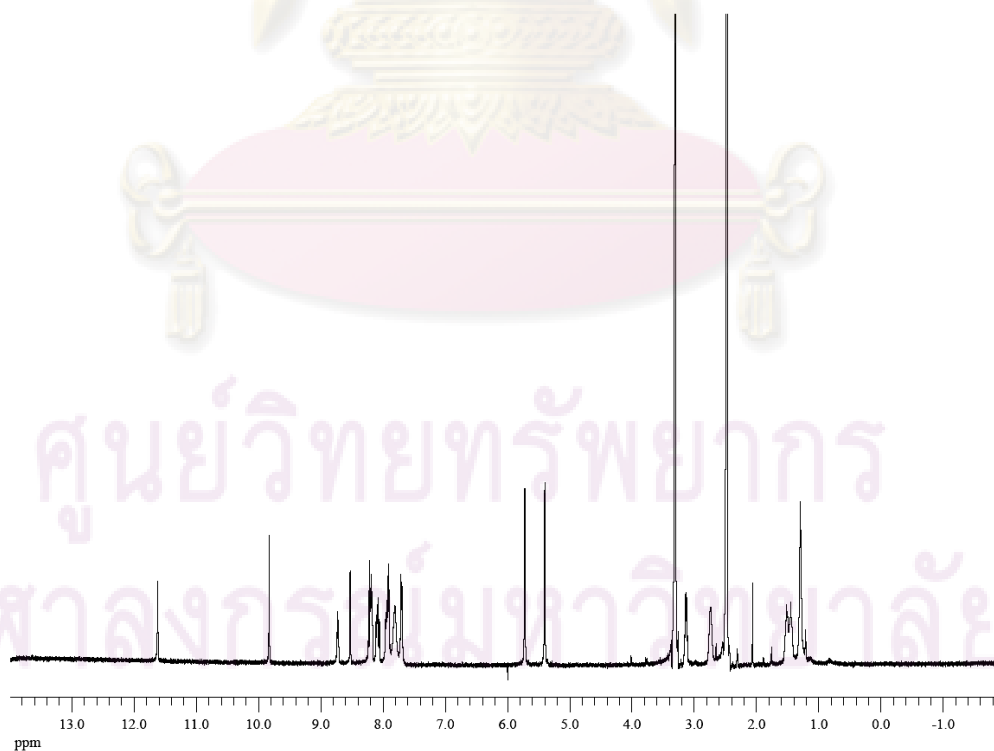
Figure A.3 The ^{1}H-NMR spectrum of *tert*-butyl 3-aminopropylcarbamate **(3)** in CDCl$_3$ with 400 MHz.

Figure A.4 The ^{1}H-NMR spectrum of *tert*-butyl 3-(2-chloroacetamido)propylcarba-mate **(4)** in CDCl$_3$ with 400 MHz.

Figure A.5 The ¹H-NMR spectrum of Boc-ligand containing anthraquinone and imidazole moieties **(5)** in DMSO-d6 with 400 MHz.
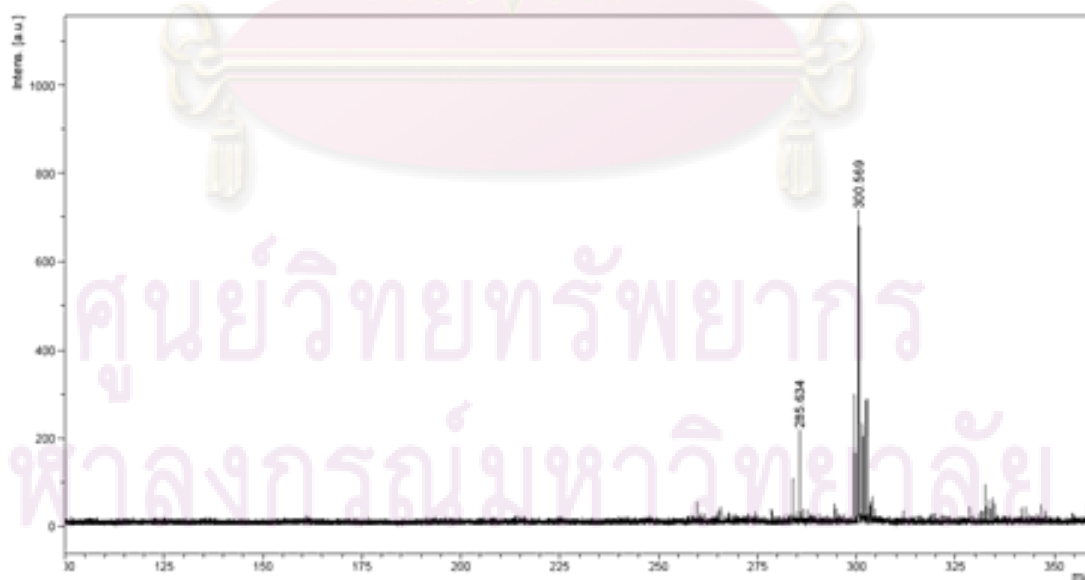

Figure A.6 The ¹H-NMR spectrum of ligand **L1** containing anthraquinone and imidazole moieties in DMSO-d6 with 400 MHz.
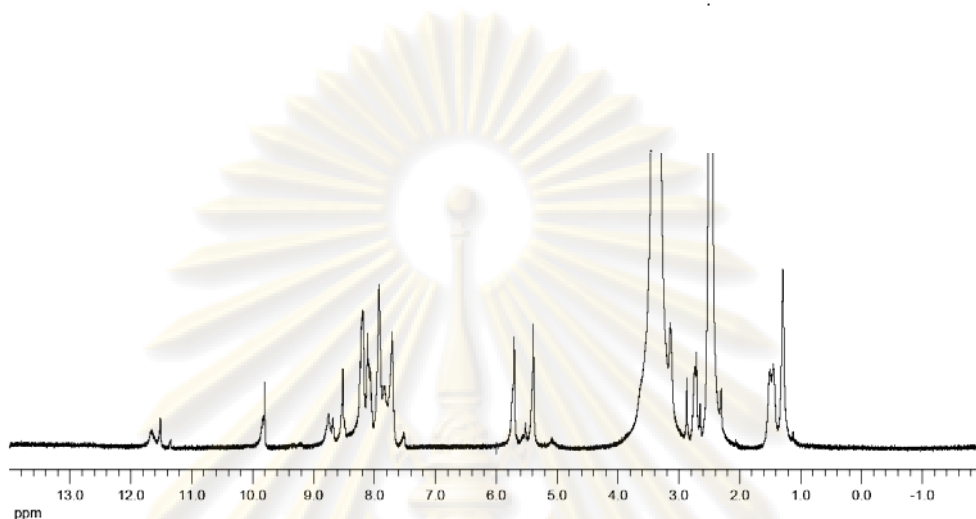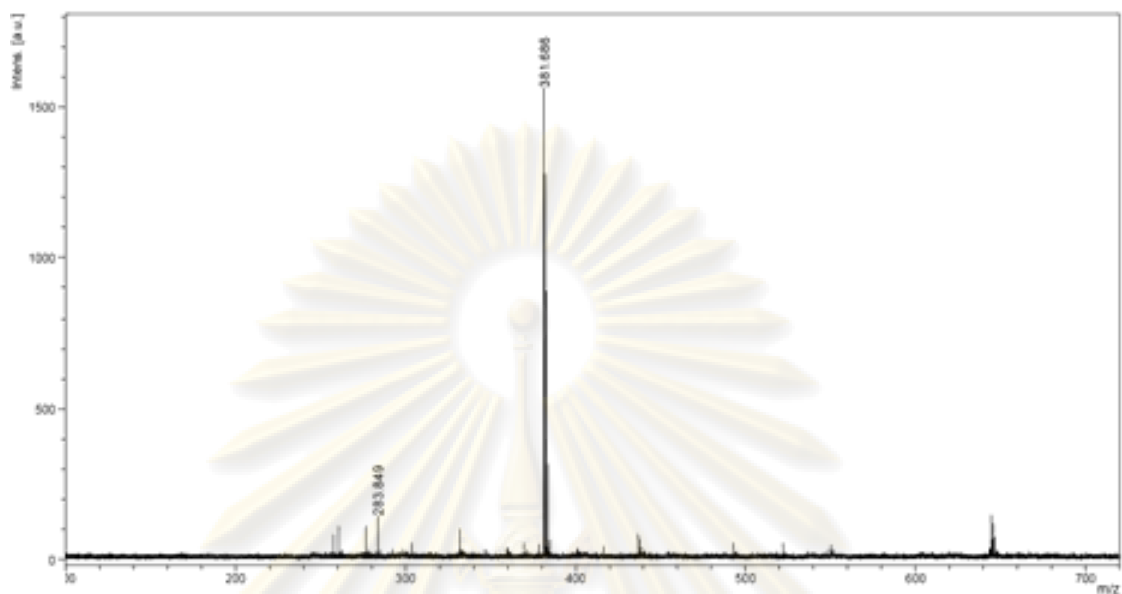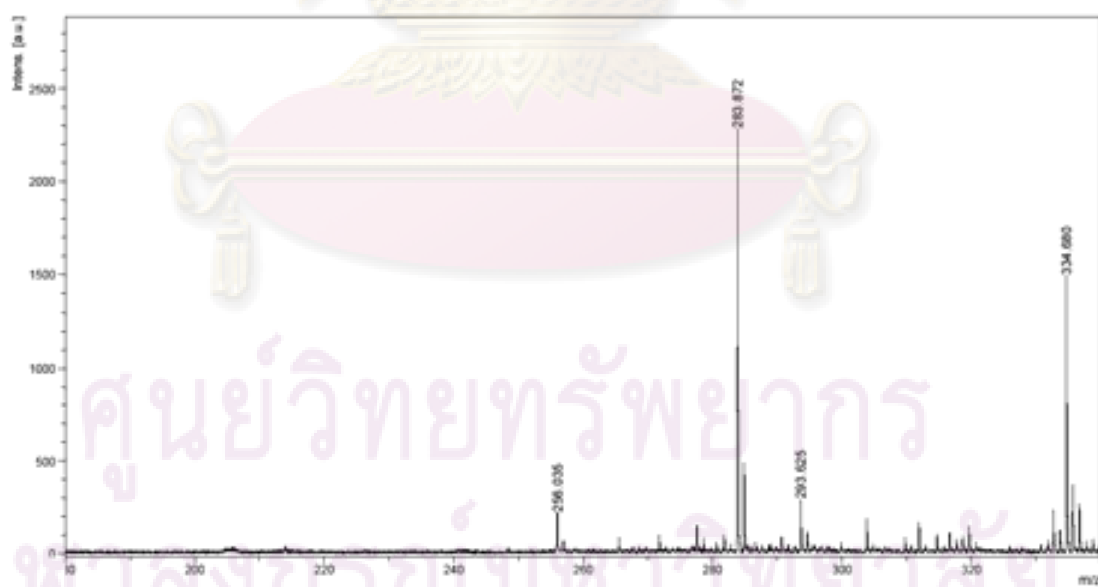
Figure A.7 The ^{1}H-NMR spectrum of ligand **L1** modified MWNTs in DMSO-d6 with 400 MHz.
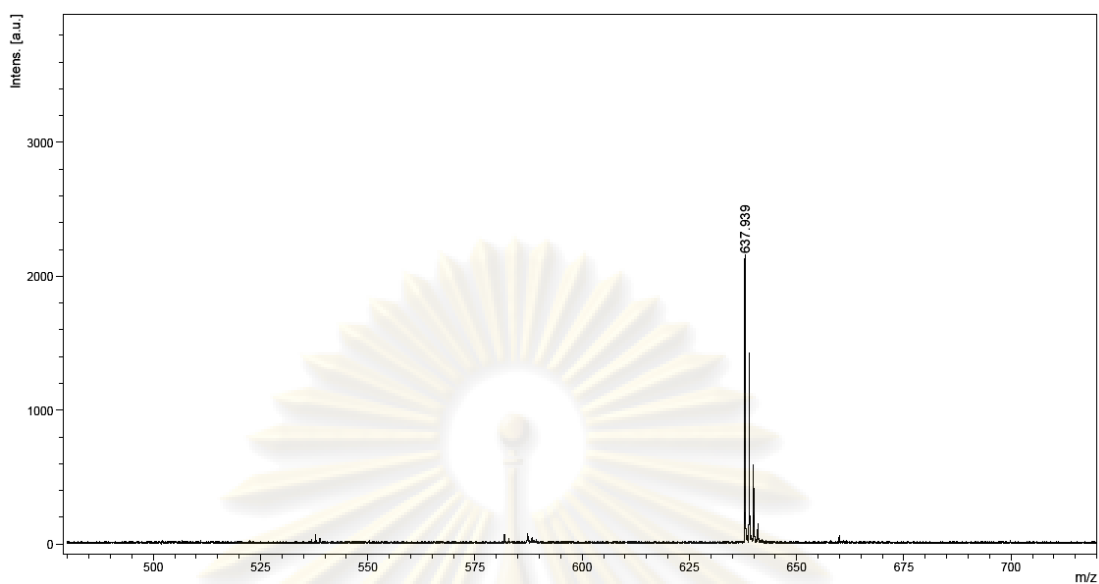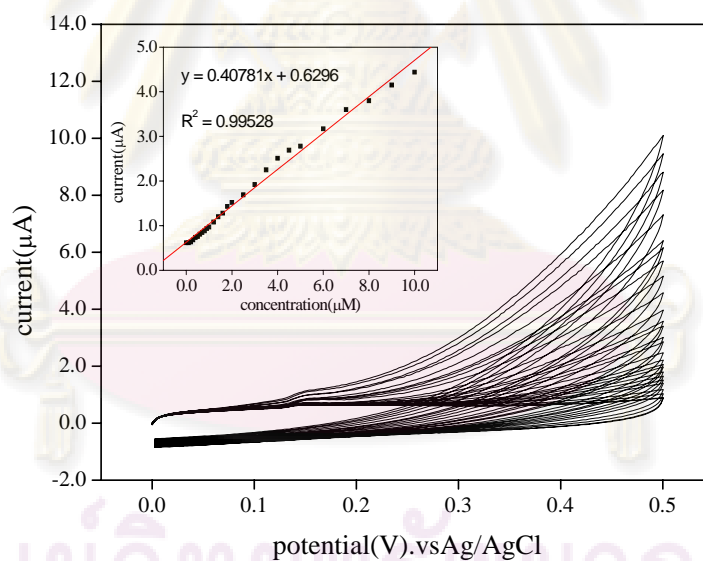

Figure A.8 MALDI-TOF mass spectrum of **(1)**.

Figure A.9 MALDI-TOF mass spectrum of **(2)**.

Figure A.10 MALDI-TOF mass spectrum of **(4)**.

Figure A.11 MALDI-TOF mass spectrum of **(5)**

Figure A.12 Cyclic voltammograms of **L1**/MWNTs modified GC electrode in pH 7.0 buffer solution (HEPES + NaCl) at different concentration of hydrazine (0.0-10.0 μM), scan rate 100 mVs^{-1}. Inset shows the variation of the electrocatalytic current vs. the concentration of hydrazine (Exp II).

Table A.13

Intercept, slope, correlation coefficient, standard deviation and detection limit for hydrazine detection at **L1**/MWNTs modified GC electrodes.

Exp	A	B	R^2	SD^a	DL^b
I	0.89221	0.53443	0.99570	0.18502	1.04
II	0.62960	0.40781	0.99528	0.13192	0.97

$y = A + B*x$

[a] Standard deviation of blank (five values were estimated).

[b] Detection limit (μM).

VITA

Miss Machima Manowong was born on August 1, 1983 in Chiangmai, Thailand. She received her Bachelor degree of Science in Chemistry from Chiangmai University in 2004. Since 2005, she has been a graduate student at the Department of Chemistry, Chulalongkorn University and become a member of the Supramolecular Chemistry Research Unit under the supervision of Associate Professor Dr. Thawatchai Tuntulani and Assistant Professor Dr. Boosayarat Tomapatanaget. She finished her Master's degree of Science in the academic year 2008.

ศูนย์วิทยทรัพยากร
จุฬาลงกรณ์มหาวิทยาลัย